Raman Endoscopy Using Optical Fiber Technology

João Marques
Mestrado em Física
Departamento de Física e Astronomia
2021

Orientador
Dr. Orlando Frazão, Instituto de Engenharia de Sistemas e Computadores, Tecnologia e Ciência

Coorientador
Dr. Susana Silva, Instituto de Engenharia de Sistemas e Computadores, Tecnologia e Ciência

U.PORTO

FACULDADE DE CIÊNCIAS
UNIVERSIDADE DO PORTO

Todas as correções determinadas pelo júri, e só essas, foram efetuadas.

O Presidente do Júri,

Porto, _____/_____/_____

UNIVERSIDADE DO PORTO

MASTERS THESIS

Raman Endoscopy Using Optical Fiber Technology

Author:
João MARQUES

Supervisor:
Orlando FRAZÃO

Co-supervisor:
Susana SILVA

A thesis submitted in fulfilment of the requirements
for the degree of MSc. Physics

at the

Faculdade de Ciências da Universidade do Porto
Departamento de Física e Astronomia

December 23, 2021

" Remember to look up at the stars and not down at your feet. Try to make sense of what you see and wonder about what makes the universe exist. Be curious. However difficult life may seem, there is always something you can do and succeed at. It matters that you don't just give up. "

Stephen Hawking

Acknowledgements

The author has enjoyed the company and support of many people throughout the journey from which this document is the result. He would like to thank every one of his colleagues, professors, family, and friends. He would also like to give special attention to those that, in some way, helped him overcome difficulties or provided the necessary encouragement when he needed the most.

First, the author would like to thank his Supervisor, professor Orlando Frazão, and Co-supervisor, Dr. Susana Silva for always believing in him and trusting his work. Beyond their continued support, advice, and guidance, they provided the author with key opportunities in various occasions.

Second, the author would like to express his gratitude to Dr. Susana Novais for her availability and assistance, right from the beginning of the laboratory work. Her experience and continued presence were crucial for a fast initial development, without which the success achieved would not be possible.

The author would also like to show his appreciation to Catarina Monteiro and António Vaz. Their proficiency in laboratory work and their insights, provided the solution to practical problems more than once.

The author is indebted to INESC TEC and to IFIMUP/IN for admitting him and providing the indispensable conditions and access to state-of-the-art equipment.

The members of the SPIE Chapter deserve special mention for the productive discussions, from which the solutions to technical problems also derived and for their fellowship.

To Inês Carvalho, Sara Freitas and João Silva, the author would like to extend his friendship and kind words of fondness. For the countless hours of laboratory work, for the delightful conversations, laughs, and stress shared along this past year.

Last but not least, the author would like to reserve his biggest thank you, and express his unconditional love for his parents, Américo Marques, and Margarida Ferreira. It took a long time to get here and without their support, effort, and encouragement this document would never come to be.

This work was financed by the ERDF European Regional Development Fund through the Operational Programme for Competitiveness and Internationalization - COMPETE 2020 Programme and by National Funds through the Portuguese funding agency, FCT

- Fundação para a Ciência e a Tecnologia within project ENDOR - Endoscope based on New Optical FiberTechnology for Raman Spectroscopy (POCI-01-0145-FEDER-029724).

UNIVERSIDADE DO PORTO

Abstract

Faculdade de Ciências da Universidade do Porto
Departamento de Física e Astronomia

MSc. Physics

Raman Endoscopy Using Optical Fiber Technology

by João MARQUES

In this dissertation, the fundamentals of Raman fiberscope design are explored, and a prototype system is assembled. A brief overview of the evolution and state-of-the-art of the field is given, followed by the presentation of a simple but informative model for inelastic light scattering in molecules. The light guiding mechanisms of conventional and Hollow Core Photonic Crystal Fibers, and some of the main probe tip designs used today are covered. Applications of the technology, with emphasis in the clinical and biomedical fields are highlighted. The advantages Hollow Core Photonic Crystal Fibers have over Single Mode Fibers for the delivery of the excitation laser are brought to light by a power sweep and by a measurement of curvature sensitivity. The beam output by a cleaved tip is characterized by tracing its longitudinal, transverse and angular profiles, benchmarked by a commercial fiber bundle. Several configurations for the collection channel, with different numbers of collection fibers are studied by mapping the evolution of the collected power. A simple and inexpensive probe tip was fabricated, and a prototype system was assembled with commercially available and custom, 3D printed, parts. Preliminary measurements of Silicon and Paracetamol samples are performed. A solution for the integration of filters is included into the collection channel and characterized. Raman spectroscopy with state-of-the-art equipment was performed for the collection of reference spectra. Validation of the prototype will be deferred to future work; however, important know-how was acquired and promising results achieved.

UNIVERSIDADE DO PORTO

Resumo

Faculdade de Ciências da Universidade do Porto
Departamento de Física e Astronomia

Mestrado em Física

Endoscopia de Raman Utilizando Tecnologia de Fibra Ótica

por João MARQUES

Nesta dissertação, os fundamentos do desenvolvimento de endoscópios de Raman são explorados e um protótipo é construído. É dada uma visão geral acerca da evolução e do estado da arte da área, seguida pela apresentação de um modelo simples, mas informativo, para a dispersão inelástica da luz por moléculas. São cobertos os mecanismos de condução da luz em fibras convencionais e em fibras de cristal fotónico com núcleo oco, assim como algumas das principais arquiteturas de sondas. Aplicações da tecnologia são apresentadas, com especial ênfase aos campos médico e biomédico. As vantagens que as fibras de cristal fotónico com núcleo oco têm sobre as fibras multimodo para a entrega do laser de excitação são iluminadas através de um varrimento de potência e por uma medição de sensibilidade à curvatura. O feixe emitido por uma ponta clivada é caracterizado, através do esboço dos seus perfis longitudinal, transversal e angular, que foram avaliados em relação a um feixe comercial. Várias configurações para o ramo de coleção foram estudadas através da avaliação da evolução da potência coletada. Uma sonda simples e economicamente acessível e o protótipo de um sistema foram construídos a partir de algumas peças disponíveis comercialmente e de outras produzidas à medida por impressão 3D. Foram levadas a cabo medições preliminares com amostras de Silício e de Paracetamol. Foi caracterizada uma solução para a integração de filtros no canal de coleção. Com o intuito de aquisição de espectros de referência, foi realizada espectroscopia de Raman com um equipamento topo de gama. A validação do protótipo ficará para trabalho futuro, no entanto, ao longo deste trabalho foi adquirido conhecimento importante e foram obtidos resultados promissores.

Contents

List of Figures

Glossary

RS	Raman Spectroscopy
NA	Numerical Aperture
OFP	Optical Fiber Probes
SMF	Single Mode Fiber
MMF	Multi Mode Fiber
HC-PCF	Hollow-Core Photonic Crystal Fiber
OPM	Optical Power Meter
FWHM	Full Width at Half Maximum
FC	Ferrule Core Connector
PC	Physical Contact Connector
APC	Angled Physical Contact Connector
OSA	Optical Spectrum Analyzer
GRIN	Graded Index
OCT	Optical Coherent Tomography
SNR	Signal to Noise Ratio
CCD	Charge Coupled Device

Chapter 1

Introduction

1.1 Motivation

In recent years, optical technologies have risen has important solutions for the study, monitoring and diagnosis of several types of health conditions. They present relevant alternatives to more established techniques by providing access to hard-to-reach areas of the patient's body and, in general, dispense the need for biopsy or chemical bleaching of target tissues. However, despite there already existing some clinical trials, many of the techniques are still in a preliminary state and additional developments are still necessary for them to reach regular clinical application. Raman endoscopy in particular, is one of the most promising solutions, due to its inherent chemical fingerprinting capabilities. Some groups have made important headway into the achievement of practical and viable systems, but challenges still remain for complete validation and widespread use of the technique. Some of the difficulties are related to the development of economical and versatile probes that provide good signal to noise ratios and quick acquisition times. This dissertation is part of the ENDOR project and stems from the necessity of cultivating the fundamental know-how for the successful development of a fiberscope system for Raman endoscopy, capabilities that integrate seamlessly into the already extensive culture of fiber optics at INESCTEC and complement other work carried out at the institute.

The author himself came to be involved in such an endeavor due his previous experience with fiber optics, and his eagerness in contributing to a field where tangible contributions to society at large are possible.

1.2 Objectives

This thesis aims to explore the fundamentals of fiberscope design, laying down the groundwork and developing the know-how necessary for the achievement of a successful prototype system for Raman endoscopy.

It aspires to do so by:

- Exploring the physical basis of inelastic light scattering.
- Studying the light propagation mechanisms in different types of optical fibers.
- Informing about optimal choices for delivery and collection of light.
- Characterizing the profile of a beam output by a cleaved fiber end.
- Developing and fabricating a probe.
- Understanding the essential components for a functioning system.
- Assembling and validating a fiberscope prototype.
- Providing hands-on experience with a state-of-the-art confocal system as reference and a means of additional instruction.

1.3 Thesis Structure

The introductory chapter of this thesis contains the motivation and the objectives behind it, followed by the outline of its structure. It ends with a list of outputs derived from the reported work.

The second chapter begins by providing an overview of the evolution and state-of-the-art of the field. Starting in the earliest reports the author was able to find, it provides insight into what problems lead to the production of the initial probes. An effort to follow the main experimental and theoretical developments that allowed the continuous improvement of the probes was made. It was also paid close attention to the main actors responsible for the validation and credibility of the technology. The different stages of evolution are referenced and the integration with other spectroscopic techniques is also presented. The state-of-the-art review ends, by presetting some of the most recent advances and achievements. Next, the processes behind the different types of inelastic scattering of light are explored by the presentation of a simple but informative model,

bringing some sensibility of the physics involved. This is followed by a presentation of light guiding mechanisms in solid and hollow core fibers, and of some of the most prominent probe architectures. Chapter 2 ends with a survey of applications of the technology, with particular emphasis to the clinical and biomedical fields.

Chapter 3 contains much of the experimental work performed along this thesis, being effectively its core. It is divided in three main sections. Its first section describes a power sweep that informs about which of the fibers has the lowest losses, and a measurement of the curvature sensitivity of the two fiber types. The second encompasses the characterization of the beam emitted by a cleaved tip of HC-PCF, trough the tracing of its longitudinal, transverse and angular profile. The third delineates the development and fabrication of the probe tip, presenting the study of collection branch configurations, and the fabrication process. Custom parts, produced by 3D printing are described, and the filter holder is characterized. This chapter is capped with a description of the final prototype and of preliminary measurements of Silicon and Paracetamol samples.

The last chapter of experimental work has only two sections, where the Renishaw spectrometer, the procedures employed for the collection of reference Raman spectra, and the spectra acquired are described.

The dissertation ends with a summary of the results gathered and proposals of future work. The Appendices contain the description of a 3D printed support piece, specifications of the fibers used along the reported work, a graphic, and a table of the spectrum of Paracetamol. The document itself terminates with a list of references consulted and mentioned.

1.4 Outputs

- J. Marques, S. Novais, S. Silva, and O. Frazão, "Characterization of an Hollow Core PCF for Endoscopy Applications: A Proof Concept," in 2021 Telecoms Conference (ConfTELE). Leiria, Portugal: IEEE, Feb. 2021, pp. 1–5. [Online]. Available at: https://ieeexplore.ieee.org/document/9435477/.

- J. P. F. Marques, S. Novais, S. Silva, and O. Frazão, "Evolution of the detected luminous power with the increase of the number of collection fibers for application in Raman Endoscopy", Scientific Poster presented at Optics and Photonics for the Scientific Progress, University of Kent (UK), Apr. 2021.

- J. Marques, “Raman Endoscopy Using Optical Fiber Technology”, presentation at Jornadas da Engenharia Física, Física e Astronomia”, Porto, Portugal, Mar. 2021.
- J. Marques, ”Fundamentals in Raman Fiberscope Design”, presentation at UP SPIE Chapter - Student Talks, Porto, Portugal, Dec. 2021.

Chapter 2

Review

This chapter begins with a brief overview of the evolution of the field of optical fiber probes for Raman endoscopy, from early beginnings to the state of the art.

The second section is itself subdivided in three subsections related to the main background knowledge the work carried out entails. A simple model for Raman scattering is presented in order to provide some sensibility about the physical processes involved and how they relate to the type of spectra this technique provides. Next, a description of the different types of optical fibers used along the work and a brief overview of the light guiding mechanisms involved is given. The section ends with a summary of the most relevant probe tip designs today. The chapter closes with a brief outline of some of the applications this technology, highlighting the clinical and biomedical fields.

2.1 State of the art

As far as the author was able to determine, the works of Eysel (1971) and of A. Eckbreth (1979) represent the earliest reports of the usage of optical fiber probes for the collection of Raman spectra. In these works, fiber optics rise as a solution for the collection of spectra in geometries different from those available at the time or, for the isolation of sensitive equipment from the area where the spectra where being generated [2, 3]. The first account of the usage of fiber probes for both the delivery of the excitation laser and collection of the Raman signal, emerged in a publication from 1980 by G. R. Trott and T. E. Furtak [1]. The authors describe the setup presented in Figure 2.1, which allows the insertion of two fiber bundles in discrete angles for the achievement of Angular Resolved Raman Spectroscopy, however, in this case the emission and collection probes were separated.

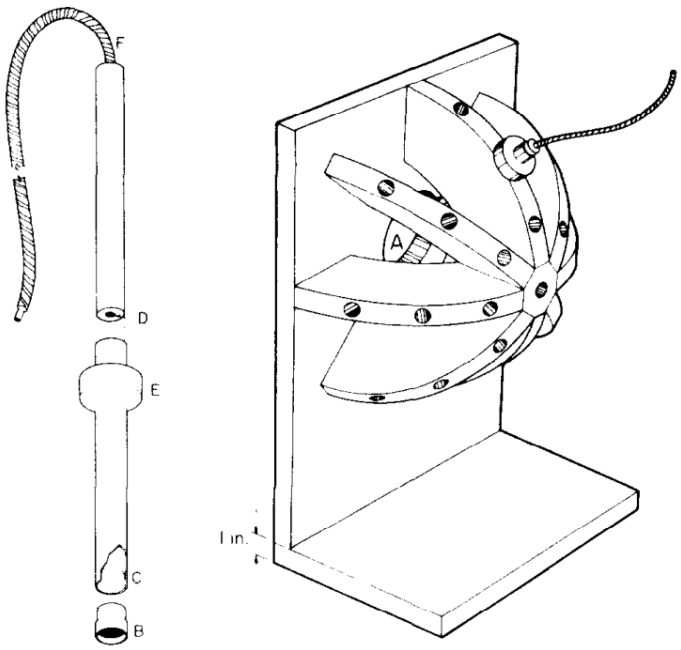

FIGURE 2.1: Schematic of the probes and setup for Angular Resolved Raman Spectroscopy built by Trott and Furtak. Adapted from [1].

The earliest account of a probe which integrates the emission and collection fibers, built for the purpose of collecting Raman spectra, that the author was able to find appears in a paper from 1983, by Richard L. McCreery and Martin Fleischmann [4]. During the remaining of the decade, McCreery, Schwab and their colleges appear to be the main actors, laying out much of the groundwork in the design and fabrication of initial optical fiber Raman probes, presenting results that validated and legitimized the technique.

At this point, the probes consisted mainly of cleaved fiber tips, packed in a N around one geometry. Some attempts at using the same fiber for excitation and collection quickly conclude that this option is less viable than a multi-channel solution due to the drowning of the sample's Raman signal by the silica's background [5–9]. During this time, Plaza [10], Hendra et al. develop theoretical and practical models for the parameters relevant for a successful probe, cementing the development of the field in a more solid foundation. The two-part work published by Hendra and his co-workers is of particular relevancy[11].

In the 1990's, continuing his previous work, McCreery teams up with C. Allred and Newman for the demonstration of the advantages of using the optical fiber probes with a CCD based spectrograph and NIR (1064 nm) excitation wavelengths. In their reports, they show that, for both liquid and solid samples, the optical fiber probes achieve similar performance to the one achieved by a more traditional assembly and that the NIR excitation

provides advantages over visible wavelengths, avoiding the excitation of fluorescence [12, 13]. Myrick and Angel published two articles which provide a thorough analysis of the performance of several configurations of optical fiber tips with regards to luminescence and Raman spectroscopy [14, 15]. From this point on filters become an important part of the design of this type of optical systems, being present in almost all designs from this paper onward. Other projects bring advances in the practicality of the optical fiber systems for biological, clinical, and other environmentally challenging situations [16–20].

In 1996, three landmark works are published. Cooney et al. publish an extensive, two-part, study of the different probe tip designs conceived to that date. They present theoretical calculations of several relevant parameters related to their performance in different environments and then demonstrate their validity through the characterization of several samples of those designs [21, 22]. Lewis and Griffiths publish a major review of the advances on the construction and design of optical fiber probes for Raman spectroscopy. Much of the work mentioned above is cited, along other complementary references [23]. Mahadevan-Jansen and Richards-Kortum deliver a major review of the evolution of Raman spectra of biologically relevant molecules for the development of cancer tissue. The extensive analysis provided by these three papers is still relevant today and provides valuable information. That same year, Ma et al. provide additional insight about the origins of the background Raman signal and which fiber parameters help in its reduction[24].

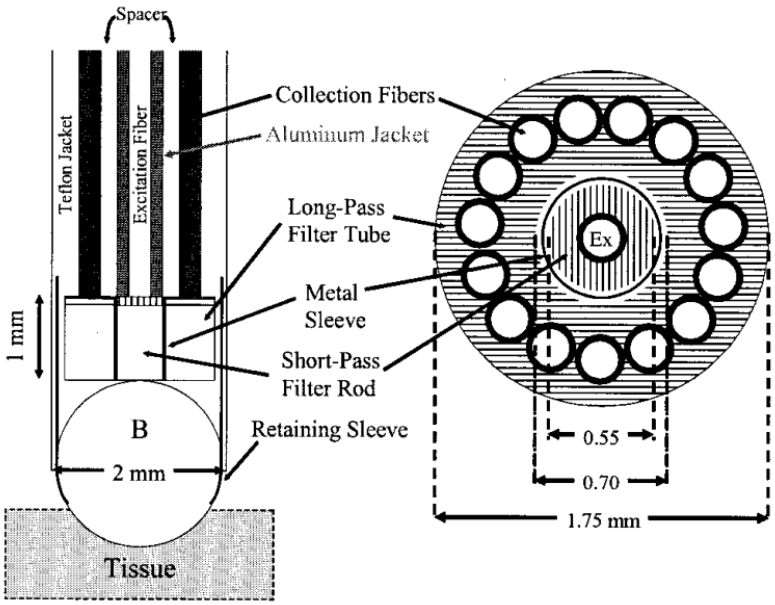

FIGURE 2.2: Schematic of a probe head which includes filters and a ball lens. Adapted from [25].

From here, the number of groups involved in the field increases dramatically, with many focusing on the improvement of the Signal to Noise Ratio (SNR) of the systems and in their application to life sciences. The N around 1 type of designs endure [26–30], however, evolutions and different solutions also come to light. Some of these are presented in section 2.2.3, however, two should be highlighted here. First, Mahadevan-Jansen et al. [31], reveal an architecture that keeps the emission and collection channels apart, resorting to a mirror to deflect the excitation beam into the focus spot of the collection lens. Second, the introduction of a ball lens in front of the cleaved fiber ends is also proposed and built[25, 32]. A schematic of this architecture can be seen in Figure 2.2.

The next big step comes with the introduction of Hollow-Core Photonic Crystal Fibers (HC-PCF) [33]. Among other advantages, these fibers bring the promise of probes nearly free of the background Raman signal inherent to Silica. Komachi and Konorov are at the forefront of this development, constructing and testing several probes with these new fibers, however, others also explore them [29, 34–38].

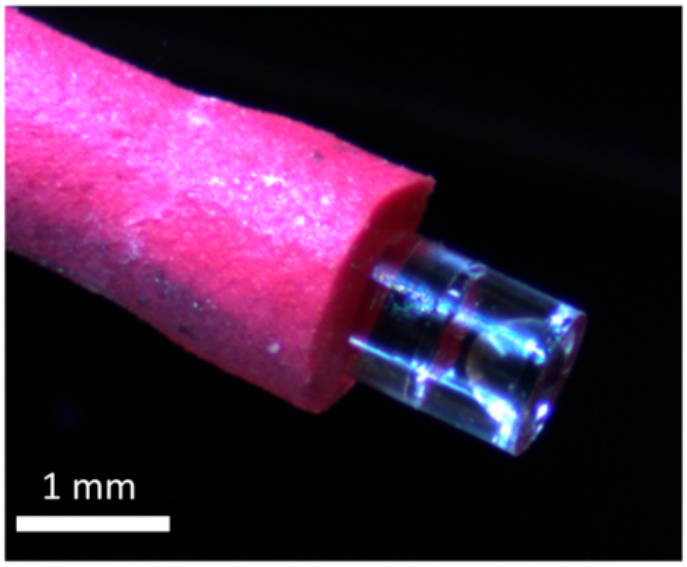

FIGURE 2.3: Photograph of the micrometric distal end of a probe achieved by Ross et al. Adapted from [39].

The last five years have given rise to multimodal probes which provide a combination of Raman spectroscopy with other techniques, such as Autofluorescence and Diffuse Reflectance [38, 40–44], to the usage of negative curvature fibers [45], to the inclusion of self-synchronized fiber lasers [46] and to the miniaturization of the probes [39, 47]. An example of which can be seen in Figure 2.3.

2.2 Raman Endoscopy System Design

2.2.1 Raman Scattering

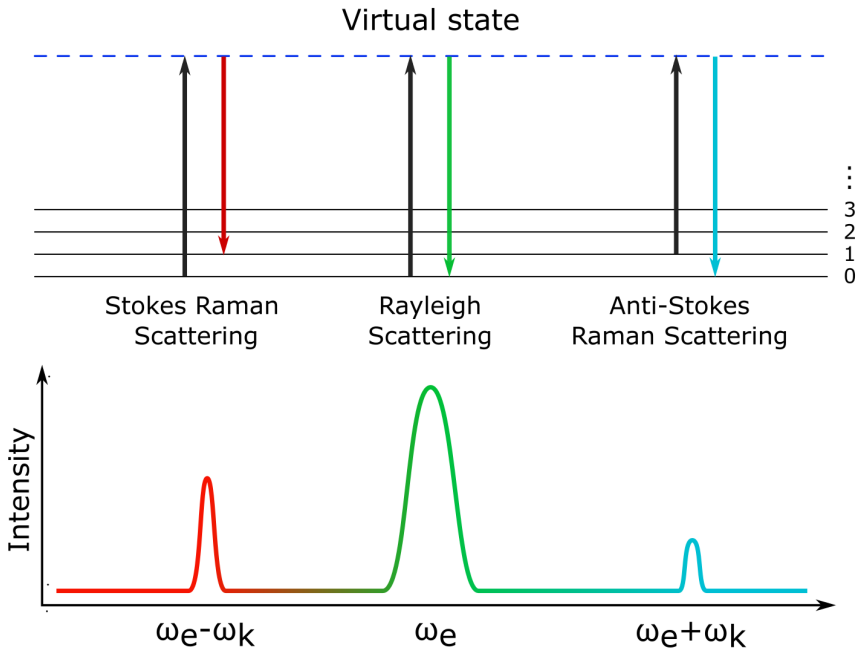

FIGURE 2.4: Schematic of the different types of light scattering.

Discovered in 1928 by C. V. Raman and K. S. Krishnan, Raman spectroscopy is a technique that, due to its nondestructive nature and great capability to provide insight about the chemical composition of samples, has rapidly occupied a central role in various areas of life and material characterization sciences. It relies on the inelastic scattering of light, where energy is transferred between photons and molecular bonds, resulting in a change in both the vibrational state of the molecule and the wavelength of the emitted photons.

Adopting a simple harmonic oscillator model for the molecular bond between two atoms of different elements, this bond can be approximated as a spring with elastic constant k, between two masses M_1 and M_2. In this case, if the field's intensity is low when compared with the force that keeps the bond, the induced dipole moment perturbing the charge distribution in the molecule is given by $\vec{p} = \alpha E$, where α denotes the polarizability (a second rank tensor) and E refers to the electric field. Considering a small sinusoidal displacement of the nuclei, this term takes the form:

$$\alpha = \alpha_0 + \frac{1}{2}\frac{\partial \alpha_0}{\partial r} r_0 \sin(\omega_k t + \delta) \tag{2.1}$$

where α_0 is the polarizability at equilibrium, r_0 is the initial displacement, ω_k the frequency of one of the molecule's normal modes of vibration, t is time, and δ is a phase component. Defining ℓ as the typical largest dimension of a simple molecule, we have that for optical wavelengths, $\frac{\ell}{\lambda} \ll 1$ therefore, the optical field can be approximated as a uniform oscillating field. Putting all of this together, we get a new expression for the induced dipole moment:

$$p = \alpha_0 E_0 \sin(\omega_e t) + \frac{1}{2}\frac{\partial \alpha_0}{\partial r} r_0 E_0 \sin(\omega_k t + \delta)\sin(\omega_e t) \tag{2.2}$$

where E_0 is the electric field's amplitude and ω_e is its frequency. The first term of this expression corresponds to Rayleigh scattering, while the second represents the inelastic scattering that we call Raman scattering. Further developing this second term, we arrive at the form:

$$p_{Raman} = \frac{1}{4}\frac{\partial \alpha_0}{\partial r} r_0 E_0 \left[\cos\left((\omega_e - \omega_k)t + \delta\right) - \cos\left((\omega_e + \omega_k)t + \delta\right)\right] \tag{2.3}$$

from where it can be observed that two different inelastic scattering processes are possible. These are called Stokes and Anti-Stokes Raman scattering, respectively. In the first case, the molecule is in its vibrational ground state and energy is transferred from the photon to the molecule, placing it in an excited state and shifting the photon's wavelength to a longer one (red shift). In the second case, the molecule is already in an excited state and energy is transferred from the molecule to the photon, sending the molecule to its ground state and shifting the photon's wavelength to a shorter one (blue shift). These processes present a cross section much smaller than the ones of fluorescence or Rayleigh scattering and their intensity is usually four orders of magnitude lower, approximately. It must be noted, that since the intensity of the Anti-Stokes component depends on the population of molecules in an excited vibrational state, at room temperatures, the amplitude of this process is even lower than its Stokes counterpart.

Despite providing insight into the origins of the phenomenon of inelastic light scattering, this classical model does possess some limitations. First, it only grants qualitative analysis of the spectra, not providing a framework which allows the connection between the peak's amplitude and the transition energy. It also does not differentiate between the different types of rotations and vibrations that molecules contain. Therefore, resorting to quantum mechanics in a semi-classical approach is necessary in order to overcome these difficulties. I this case, the electric dipole moment and the polarizability tensor are

replaced with a transition electric dipole moment and a transition polarizability tensor. Then, Time Dependent Perturbation Theory is used to find the wave functions of the several energy states that the molecules can occupy, resorting to symmetry tools to determine the selection rules and find which transitions are Raman active. This approach solves most of the shortcomings of the classical model and it is the *de-facto* standard in current practice.

Due to the fact that the author wishes to limit the scope of this dissertation to furnishing the reader with sensibility to physics involved, he advises the curious reader to refer to [48] for a more extensive introduction or to [49] for an exhaustive and unified treatment of the matter.

Due to the fact that the energy of a bond is directly correlated to the frequency at which it vibrates, and that the Raman signals appear as a shift in the energy of the incident photons, it is common practice to represent the spectra in units of inverse wavelength, relative to the excitation one. This allows for a more direct comparison between spectra acquired with different excitation wavelengths. The conversion to these units is given by:

$$\frac{\Delta\nu}{cm} = \left(\frac{1}{\lambda_0(nm)} - \frac{1}{\lambda_p(nm)}\right)\frac{10^7}{cm} \tag{2.4}$$

2.2.2 Optical Fibers

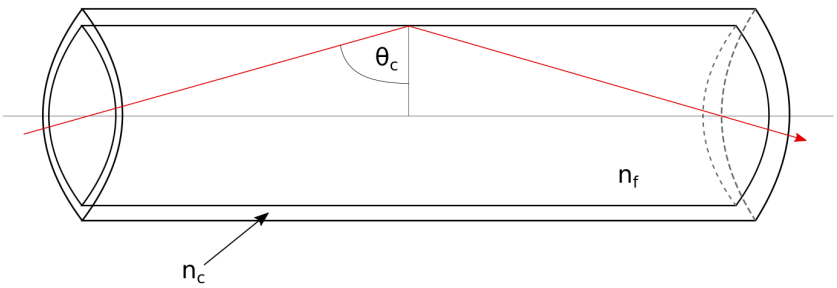

FIGURE 2.5: Total internal reflection in a solid core fiber.

Optical fibers consist of long filaments, typically made out of silica or plastic, which act as waveguides for light. They comprise a core, where light travels, and a cladding which provides isolation and protection. Usually, the cladding's refractive index is lower than the one from the core, making it possible for light to suffer total internal reflection when it meets the interface between the two sections. In relation to the normal to this interface, the maximum incidence angle for total internal reflection to occur can be determined directly

from Snell's Law as depending on the ratio between the refractive indices of the core and of the cladding, being given by the following expression:

$$\theta_C = sin^{-1}\left(\frac{n_c}{n_f}\right) \tag{2.5}$$

where θ_C is the critical angle and, n_f and n_c are the refractive indices of the core and of the cladding, respectively. Light satisfying this critical angle propagates along a solid core fiber with very low losses over long distances, however, if the fiber presents curvature, this geometric condition might stop being satisfied, causing light to diffract into the cladding, incurring in losses. Other loss mechanisms include scattering, absorption, impurities, and micro fractures present in the core's structure.

The Numerical Aperture (NA) of optical fibers is given by:

$$NA = \sqrt{n_f^2 - n_c^2} \tag{2.6}$$

and provides an alternative way of expressing the critical angle, however, it also informs about the acceptance angle, which defines the vertex of the cone of light that can enter the fiber and propagate. In turn, each entrance angle determines a particular transverse energy distribution, corresponding to a *mode* of propagation. Depending on the number of modes possible, the guides are distinguished into *single mode* or *multimode* fibers.

Despite this being the light propagation mechanism in most common optical fibers, in the 1990's new light guiding processes were proposed, giving rise to Photonic Crystal Fibres (PCF) [33]. In this case, the cladding presents a periodic structure which produces a photonic bandgap, confining light to propagate in the core. This periodic structure can be tuned to limit the guided light to a particular wavelength band and to a singular mode. These types of fibers are also divided into two subcategories: Solid Core Photonic Crystal Fibers (SC-PCF) and, Hollow Core Photonic Crystal Fibers (HC-PCF). Of these, the HC-PCFs have found great use in Raman endoscopy due to the fact that they intrinsically eliminate most of the problems caused by the Silica's inherent background Raman signal [37, 50–53].

2.2.3 Probe tip designs

Initial Raman probes were very simple, being composed of two cleaved fiber ends, positioned parallel or in front of each other. Primary experimental and theoretical efforts for the development of fully featured probes revolved mostly in surrounding the emission

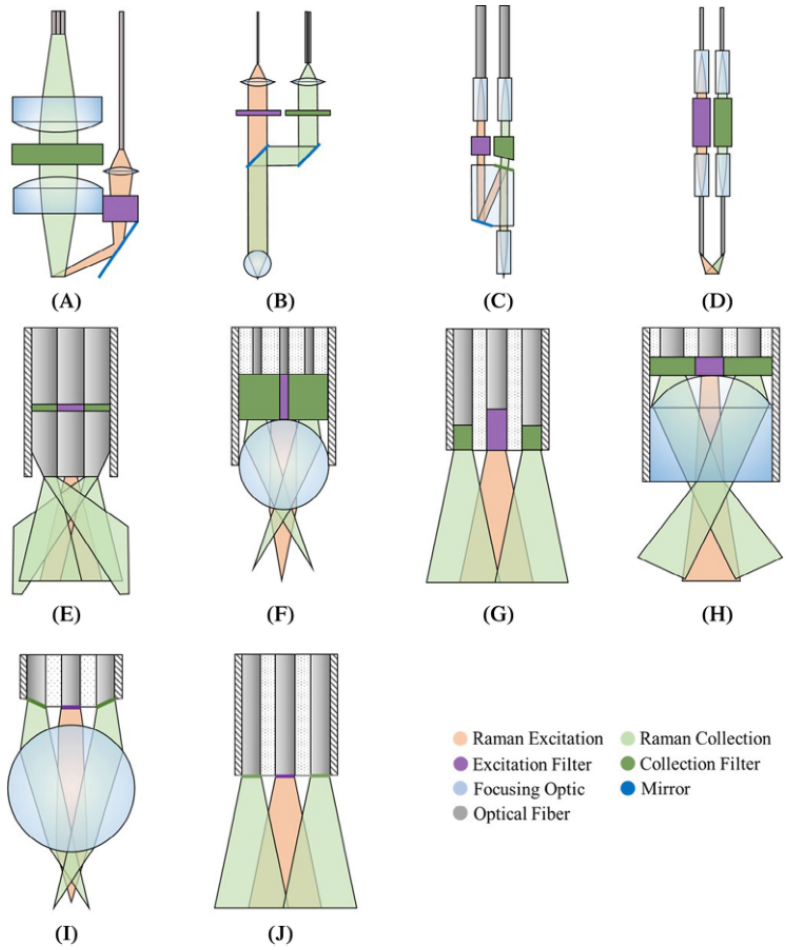

FIGURE 2.6: Schematics of different probe designs. Adapted from [54].

fiber in several layers of collection fibers with no additional optics. However, along the years, with the evolution of manufacturing techniques and with the understanding of the difficulties inherent to Raman endoscopy, many other designs were created.

Figure 2.6 shows schematics of several different constructions possible. In general, the probe designs are divided in three main groups: Volumetric, Confocal and Multimode probes [55]. The first type refers to the simplest of the probe constructions, like the one referenced above, which consist only of cleaved fiber ends and have no additional optics. The second group include ball lens, Gradient Index (GRIN) or aspheric lenses or, mirrors which allow side-viewing [56]. The third group is the one where the most complex probe designs lie, encompassing probes capable of integrating other spectroscopic techniques, such as Optical Coherent Tomography (OCT), Fluorescence, Diffuse Reflectance, and Image Guidance.

In order to control the background Raman signal generated by the excitation fiber and

to avoid the collection of the Rayleigh scattering, many of these probe designs also include filters. These filters can be integrated directly into the construction of the probe head or in a section of free space optical path, with the inclusion of a mirror, a prism, or a dichroic beam splitter, as can be seen in schematics (A), (B) and (C) from Figure 2.6. The filter at the exit of the emission fiber is usually a bandpass, while the filter at the entrance of the collection fibers is a notch filter at the chosen excitation wavelength[54].

2.3 Applications

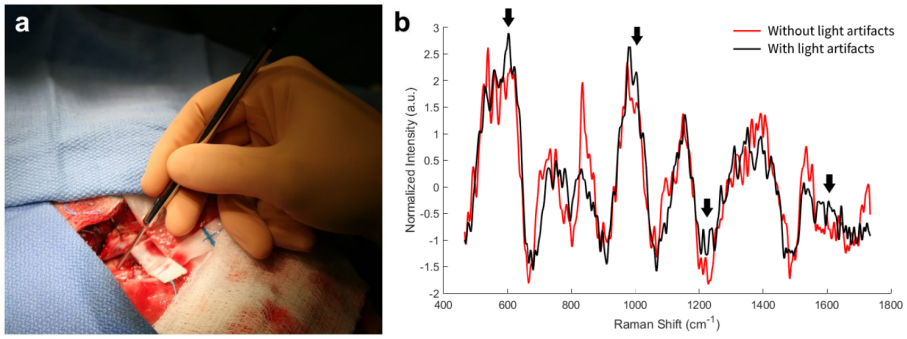

FIGURE 2.7: a) Handheld Raman probe being used for brain cancer detection during surgery. b) Spectra acquired during the procedure. Adapted from [57].

From the very first experiments, the design and construction of endoscopic systems for Raman spectroscopy is a field that aims to overcome some of the disadvantages of more traditional systems and bring the good chemical identification capabilities of the technique into more accessible and versatile instruments that can be applied to many different situations and environments. Many of the early papers already point to the potential usefulness to life sciences of this type of solutions, including, the in-vivo acquisition of spectra and the dynamical monitoring of chemical processes.

The promise of direct access to internal regions of the human body provided by these systems, associated with the diagnosis potential and to the nondestructive nature of Raman Spectroscopy, have in the last twenty years, given rise to many efforts for the development and validation of clinical solutions.

These efforts have shown that Raman Endoscopy can bring important insights when it comes to the early detection, evolution surveillance, and diagnosis of various types of health conditions.

In particular, there are already some clinical trials related to cardiovascular problems, inflammatory diseases, and several different types of cancers. During these trials, the

technique has regularly reached sensitivities above 80% and specificities of over 75%. Even better results can be obtained when multimodal systems that integrate additional techniques, such as Auto Fluorescence, Diffuse Reflectance, or OCT are employed. These allow the acquisition of additional information that can be cross referenced to improve the general accuracy of the methodology as a whole[32, 54, 55, 58–66].

2.4 Closing remarks

In this chapter, we began by doing an overview of the history of the field of optical fiber probe design and fabrication. Then, background knowledge was introduced by reviewing a simple model for inelastic light scattering, exploring the light propagation mechanisms in the different optical fiber types used, and by highlighting some of the main designs employed today. The chapter ends with a brief description of some of the applications this technology has, demonstrating that it brings relevant solutions to difficult problems.

This helped us contextualize this dissertation and provided us with basic knowledge necessary for understanding the experimental work developed in the following sections. It should be noted that, each topic could have been analyzed with greater detail, however, some compromises were necessary for brevity.

Chapter 3

Fiberscope Prototype

This chapter contains the performed experimental work that led to the development of a prototype fiberscope. It begins with a description of the different types of fibers used for each of the fiberscope's channels, followed by comparative measurements between the two types suggested for emission. The most promising fiber is then used to study the characteristics of the beam output, with the intent of understanding its profile and obtain some sensibility about the ideal sample placement. The measurements that lead to the development of an inexpensive probe tip and its fabrication process are described afterwards. The fabrication of some custom parts through 3D printing follows. The chapter ends with the characterization of a solution for the integration of filters in the collection branch, with the description of the final prototype system and some preliminary experiments.

3.1 Fibers used for the fiberscope

A complete fiberscope system consists of two separate channels for emission and collection. For delivery of the excitation laser (emission channel), two different fiber types were considered: a Single Mode Fiber (SMF, Thorlabs SMF-28) and a Hollow-Core Photonic Crystal Fiber (HC-PCF, Thorlabs HC-1060). For collection of the Raman signal, Multi-Mode Fiber (MMF, Thorlabs FG105LCA) was used. Figure 3.1 presents the cross section of two of these fiber types.

Beyond what is mentioned in section 3.1, the main physical difference between the SMF and the MMF lays in their NA. In terms of the ratio between the diameter of the core and the total diameter of the fiber, the MMF's core is much larger than the core of the

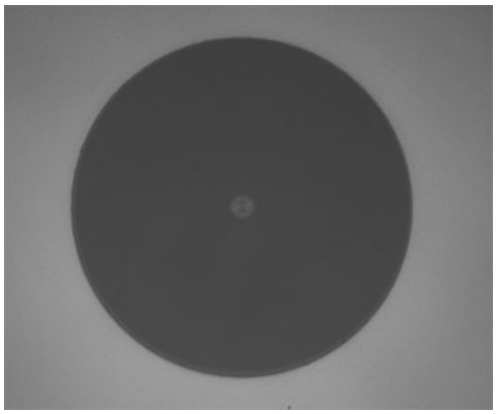

(A) SMF28 Cross section.

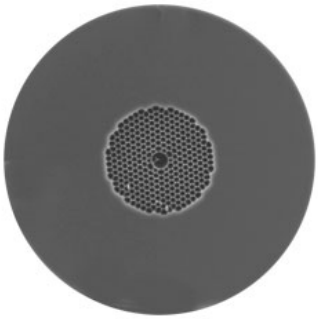

(B) HC-PCF 1060 cross section.

FIGURE 3.1: Cross Sections of the two fiber types studied. Adapted from [67].

SMF, resulting in a much larger aperture. This makes MMF ideal for collection purposes. SMF was considered for emission due to the fact that it only allows the propagation of the fundamental mode, maximizing the intensity at the center of the illumination spot. As noted in the same section, what distinguishes the HC-PCF from solid core fibers is its light propagation mechanism. While in the case of the solid core fibers, light travels along silica, in the case of the HC-PCF the core is absent, therefore light travels through air, eliminating the generation of an intrinsic Raman background signal that is present in conventional fibers.

In order to achieve optimal performance, the excitation fiber must satisfy several parameters. In this section, the power output and curvature sensitivity of the two fibers considered for emission are measured. The first measurement provided a calibration of the emitted power as a function of the laser excitation current and allowed a comparison between the samples of SMF and HC-PCF. The second permitted the determination of which of the fiber samples presents lower losses when submitted to curvature. In order to benchmark the performance of the two fibers, the power output by a RP25 fiber bundle from Thorlabs was also measured.

3.1.1 Output Power measurement

Since an indication of the laser's output power was not available on the laser driver's screen, the first measurement of the comparison between the SMF and the HC-PCF was a power sweep. Beyond allowing the creation of a power calibration curve, it had the intention of verifying which of the two fiber types allowed for the greatest output power in the excitation current range of the laser available for the experiment. This sweep was

also performed for the Thorlabs RP25 fiber bundle, which served as reference to gauge the performance of the two fiber samples. Figure 3.2 contains a schematic of the configuration setup for this measurement.

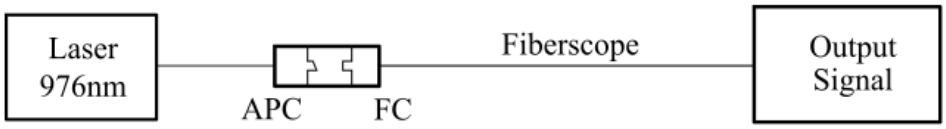

FIGURE 3.2: Schematic of the setup for the power measurement.

Each of the fiber samples had a length of approximately 2m. Both ends were cleaved and cleaned to ensure good light coupling and emission. One of the fiber ends from each sample was connectorized with a Thorlabs BFT1 and connected to a fiber coupled laser (JDSU) with a maximum output power of 460 mW, operating at 976 nm. The other end was left exposed and placed in a support which allowed alignment with a Thorlabs S302C probe, connected to a Thorlabs PM100D Optical Power Meter (OPM). In the case of the Thorlabs RP25 bundle, it was directly connected to the laser through FC/PC connectors and its emitting end was also aligned with the Thorlabs sensor.

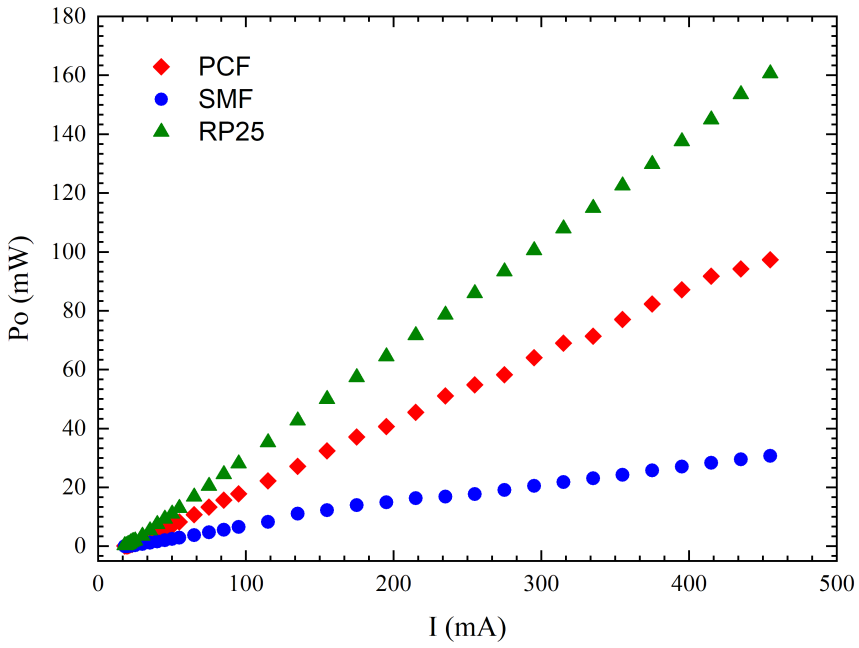

FIGURE 3.3: Evolution of output power as a function of laser excitation current for the two fiber types and the RP25 bundle.

Before performing the power sweep, the threshold current that allowed the laser to emit with reasonable power stability was determined by observing its spectrum on an

Optical Spectrum Analyzer (OSA, Yokogawa AQ6370). This threshold was established as being 18 mA. From this value, the current was incremented in steps of 1 mA until 25 mA were reached. From this point on, steps of 5 mA were applied, until the value of 455 mA was reached. The output power (Po) was measured by the OPM at each step for both fiber types and for the Thorlabs RP25 bundle. A graph of the data from this power sweep can be observed in the Figure 3.3, while the results of the linear fits can be found in table 3.1.

Sample	Slope
SMF	0.072(5) mW/mA
HC-PCF	0.229(1) mW/mA
RP25	0.3660(5) mW/mA

TABLE 3.1: Results of the linear fits performed on the data obtained during the power sweep.

It can be seen that although both the fiber samples provide less output power than the commercial solution, the HC-PCF presents an output more than two times greater than the one from the SMF across the entire excitation current range.

The lower output from the fiber samples, when compared to that of the RP25 bundle can be explained by a lower quality coupling between them and the laser.

It is useful to mention that this setup formed the foundation of most tests reported in this section and the several variations described in following sections refer mostly to the output end, where in order to enable the characterization of the emitted laser beam, several configurations of the placement of the OPM's probe and the emitting fiber tip were arranged.

3.1.2 Curvature sensitivity

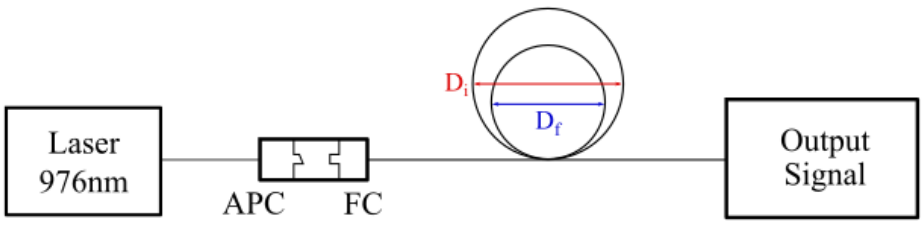

FIGURE 3.4: Schematic of the setup for the measurement of curvature sensitivity.

Some bending of the fiber cables is expected while handling a fiberscope. In regions where the fiber is curved, the angle of incidence between the light propagating in the

fiber's core and the interface between the core and its cladding might not satisfy the total internal reflection condition, incurring in light losses by dispersion. Therefore, the curvature analysis had the objective of finding which of the two fiber types presented the lowest losses when submitted to this type of deformation.

A schematic of the setup configuration is shown in Figure 3.4. It is identical to the one described in the previous section, the only difference being the single loop made half-way of the fiber sample. The diameter (D) of the loop was measured with a graduated ruler

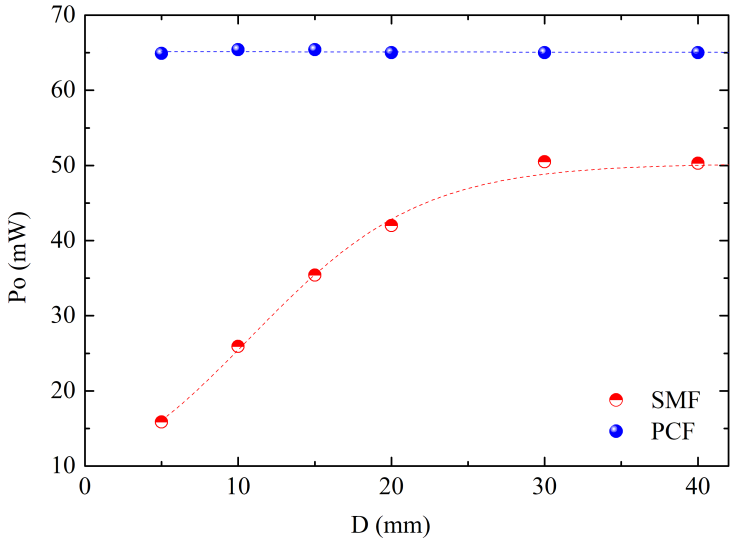

FIGURE 3.5: Results from the curvature sensitivity.

and the output power read by the OPM, for a range of diameters between 100 mm and 5 mm. During these measurements, a constant laser current of 315 mA was maintained.

The results are shown in Figure 3.5, where it can be seen that for the range between 30 mm and 100 mm, both fiber types presented negligible variation of the output signal, however, for smaller diameters, the SMF's output power started to decrease, while the PCF's remained stable, with a sensibility of only 0.0023 mW/mm.

With the results obtained from optical power analysis and curvature measurements, it was clear that the HC-PCF was a better choice for endoscopy.

3.2 Characterization of the Beam Output by the Fiberscope

In this section, we proceed to the characterization of the beam output by a cleaved tip of HC-PCF by tracing its longitudinal, transverse, and angular profile. This portrayal of

the beam serves the purpose of revealing the volume where Raman excitation is viable, informing us of the ideal sample placement in relation to the fiberscope's probe end. The same measurements were performed for the Thorlabs RP25 scope and allow for a comparison between both solutions.

3.2.1 Longitudinal profile

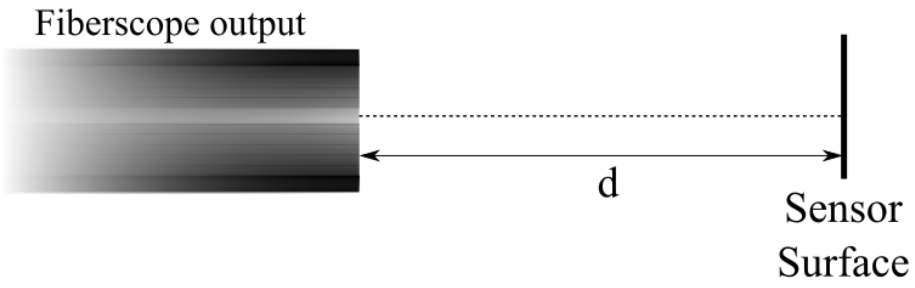

FIGURE 3.6: Schematic of the setup assembled for the tracing of the longitudinal profile.

Tracing the longitudinal profile of the beam output by the HC-PCF was accomplished by placing the Thorlabs S302C probe in a translation stage. This allowed for it to be moved in the same axis as the beam's emission direction, from 0 mm to 140 mm, by successive steps of 20 mm. In order to achieve correct power readings, vertical and horizontal alignment between the emitting tip and the probe's input aperture was ensured. The laser current was the same as the one used in the previous test. The experimental setup for this measurement can be seen in Figure 3.6, where d corresponds to distance.

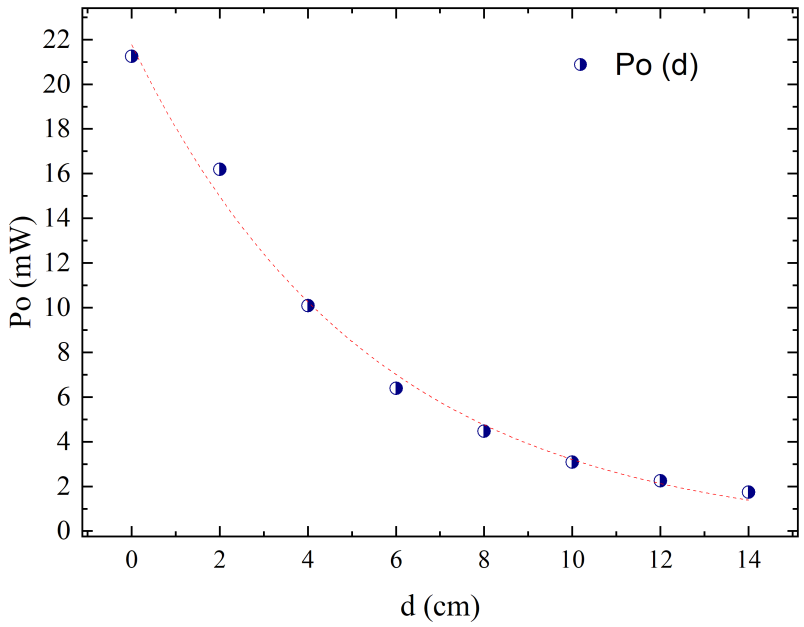

FIGURE 3.7: Exponential decay of the power with distance.

As depicted in Figure 3.6, the optical power decays exponentially with distance, presenting a decay constant of 5.41 mm, in agreement with literature [68].

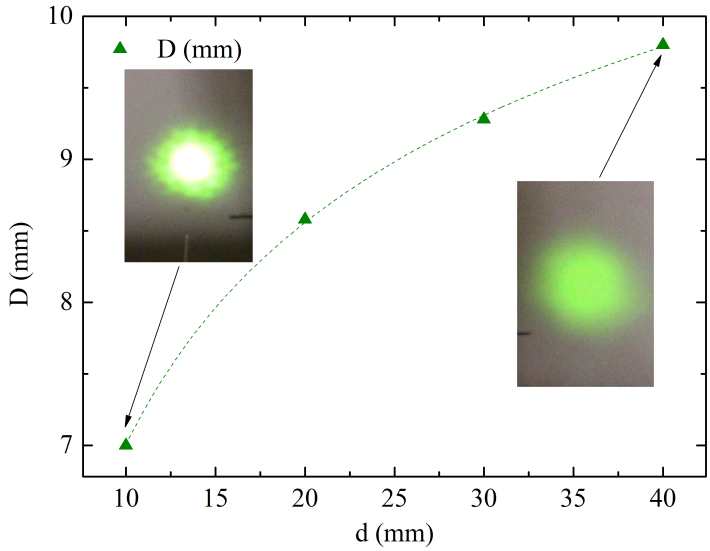

FIGURE 3.8: Graph of the evolution of the illumination spot diameter with distance.

Simultaneously, the spot's diameter was also studied. For the observation of the illumination spot, a Thorlabs VRC4 detector card was used, as presented in Figure 3.8. Photographs of the spot were taken, and its diameter was measured from the resulting images recurring to the ImageJ software. The results from Figure 3.8 show that the spot's

diameter increases in a non-linear fashion with distance. This measurement provides a visual of the evolution of the beam's size with distance. A more thorough approach would be to measure the evolution of the beam's FWHM as described in the following section.

3.2.2 Transverse profile

In this section, the measurement of the transverse profile of the beam emitted by the HC-PCF is presented.

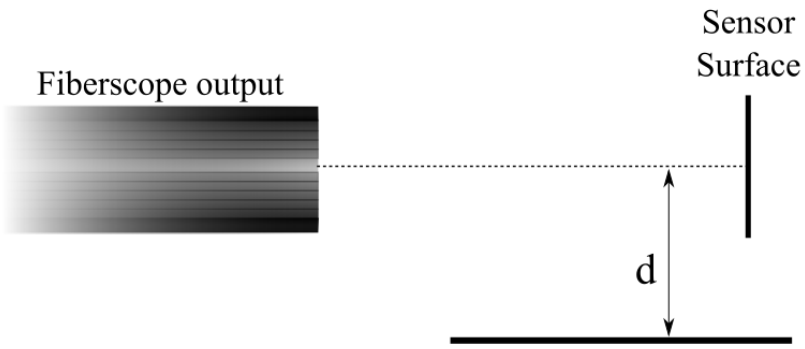

FIGURE 3.9: Schematic of the transverse profile measurement.

To this end, the OPM's probe was placed on a micrometric translation stage that allowed for it to be moved transversely in relation to the emitting fiber tip, at approximately 20 mm from its surface (see Fig. 3.9). This distance was chosen has being a typical distance to sample tissue in endoscopic applications. The position of the probe was incremented in steps of 0.5 mm and the optical power was measured at each step. The laser current was maintained at a constant value of 100 mA.

As depicted in Figure 3.10 the profile of the emitted beam is Gaussian for both cases, having a peak power of 14.81 mA and a FWHM (width at -3 dB) of approximately 9.9 mm for the HC-PCF. For the RP25 bundle, The FWHM is if 9.4 mm and the peak power was 32.72 mW This width gives an indication of the area where the optimum sample placement lies.

3.2.3 Angular profile

Figure 3.11 presents the configuration used for this measurement. As in the two previous measurements, the laser current was maintained constant at 100 mA. For this test the sensor was placed in a rotating stage, at approximately 60 mm from the output fiber.

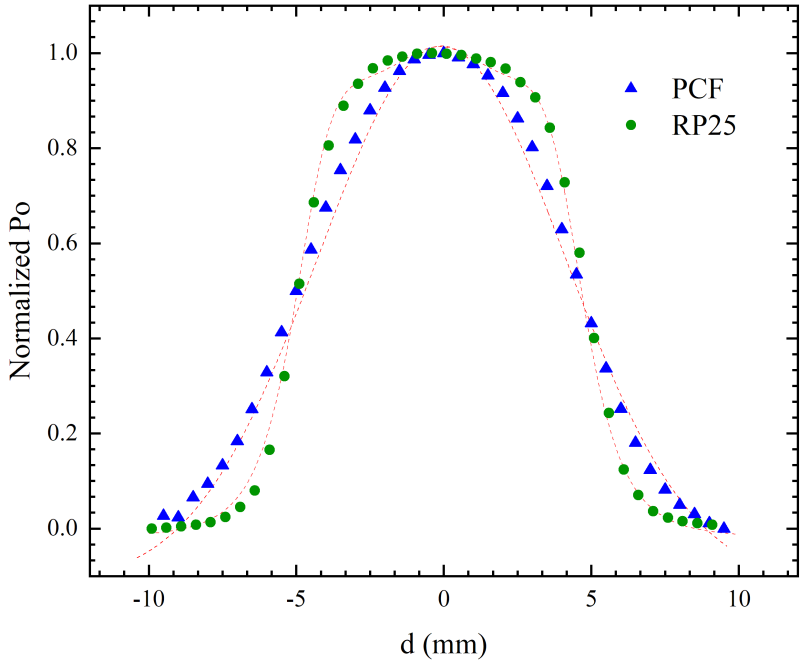

FIGURE 3.10: Transverse profile of the beam output the HC-PCF.

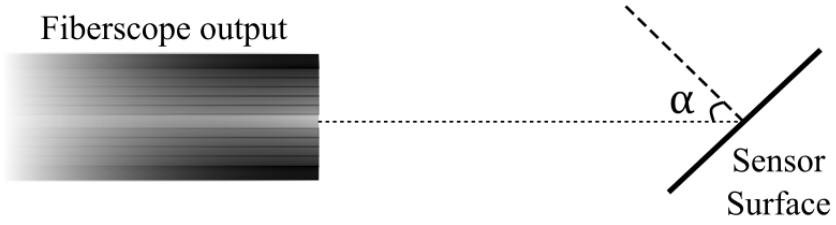

FIGURE 3.11: Setup for the angular profile measurement.

A smaller distance would be more appropriate, but this was limited by the equipment available at the laboratory.

As can be seen in Figure 3.11, the optical power was measured as a function of the angle in relation to the normal to the sensor's surface, this is what we define as incidence angle. Between 0° and 5°, the incidence angle was increased in steps of 0.5°, while in the range from 5° to 15°, it was incremented in steps of 1°.

The results from this measurement were then mirrored around 0° to generate the full profile from $-15°$ to 15°. As shown in Figure 3.12, the behavior of the power as a function of the incidence angle follows a Gaussian profile which is expected. It can also be noted that in this measurement, the angular profile of the beam from the commercial bundle is much wider, indicating that it is less sensitive to angular displacements.

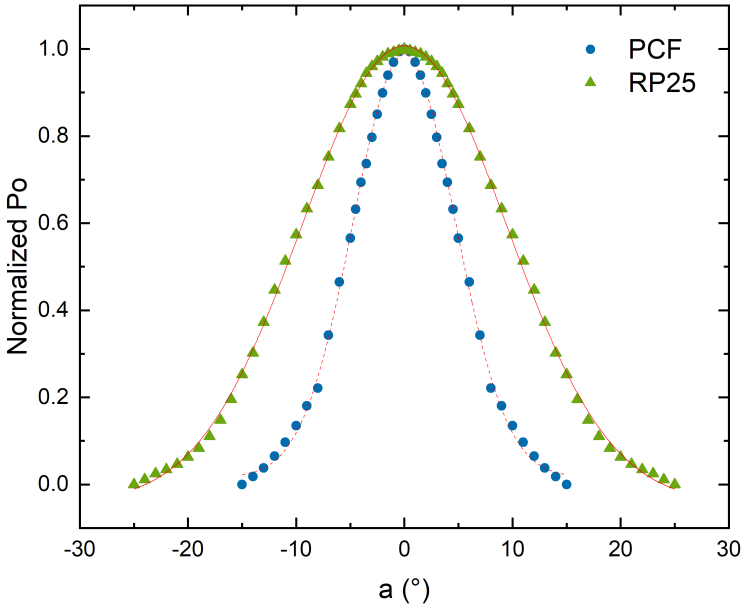

FIGURE 3.12: The beam presents a Gaussian angular profile.

3.3 Fiberscope Prototype development

From the point where the emission and collection had been studied, it was possible to transition to the development of a full fiberscope prototype. To this end, a complete probe tip had to be developed and some custom parts had to be produced.

In the following sections, measurements taken during the development and the steps necessary for fabricating the probe tip are reported. Next, the solution for the inclusion of filters which cut the Rayleigh diffraction is described and characterized. The section ends with a description and a characterization of the final prototype.

3.3.1 Dual and Multi fiber configurations

As mentioned before in section 2.2.3, probe tips that consist only of cleaved fibers (having no additional optics) can be constructed in several configurations. The simplest and more traditional designs have usually been composed of a single emission fiber, surrounded by one or several collection fibers (see section 2.2.3). In order to obtain some sensibility about the effects of increasing the number of collection fibers, we have built configurations going from 1 to 4 collection fibers and studied the evolution of the collected power and peak intensity. We were also able to compare the configurations built in-house with the previously mentioned, commercially available bundle from Thorlabs.

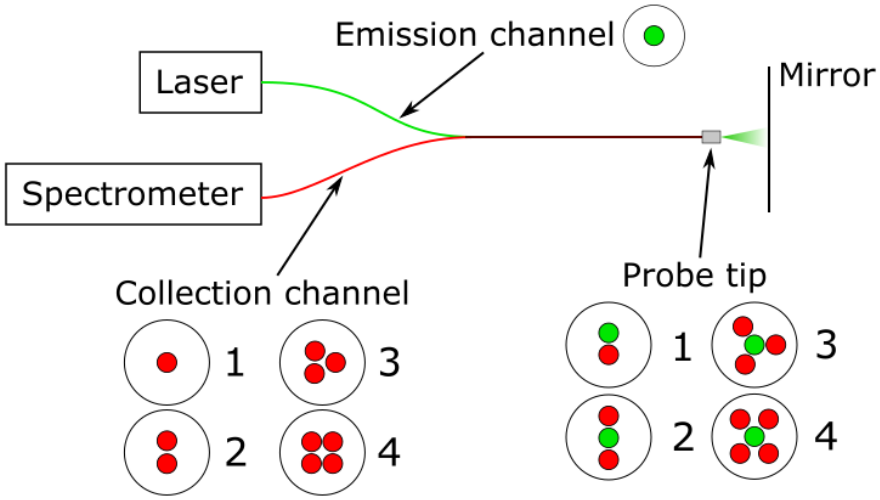

FIGURE 3.13: Schematic of the various configurations built for the study of the increase of the number of collection fibers.

The schematic of the setup for this experiment can be seen in Figure 3.13. From the results in the previous section, it was possible to conclude that the best choice of fiber for delivery of the excitation light was the HC-PCF, therefore, this was the fiber used for this purpose in all configurations reported in this section. For collection, Thorlabs FG105LCA (MMF) was used, due to its large NA of 0.22 and to its low OH content, which allow for good collection efficiency and low attenuation in the wavelength range of 800 nm to 1200 nm. Other than the fibers, the remaining equipment (laser, OPM and OSA) utilized for this experiment was the same as the one used for the measurements reported in the sections above. The laser's excitation current was maintained at a constant 130 mA throughout the experiment.

The first setup was configuration 1 from Figure 3.13 and the remaining arrangements were achieved by inserting additional collection fibers. In order to guarantee a close packing of the fibers at the probe end, they were introduced in a connector of adequate diameter from the BFT1 set from Thorlabs. The probe tip was placed in front of a mirror and the collected power and spectra were measured at the end of the collection branch. The evolution of the total collected power was studied in the conditions of suboptimal and optimal emission light coupling.

For the first case, we can observe from Figure 3.14a that the total collected power increases exponentially with the number of collection fibers, while in the second case, we can see from Figure 3.14b that the evolution is logarithmic, following an increase constant of 1.24. In the case of ideal coupling, we can observe that the total power of light collected

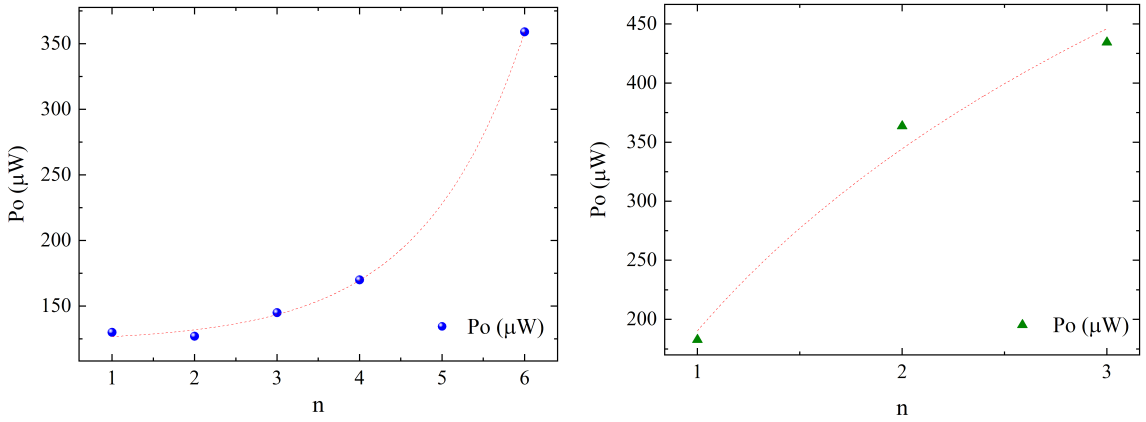

(A) Suboptimal coupling.

(B) Optimal coupling.

FIGURE 3.14: Evolution of collected power with the increase of the number of collection fibers.

by the probes built at our laboratory quickly overtakes what the commercial bundle is able to collect. Despite not having built a probe with six collection fibers, we can see that in the non-ideal case, our probes tend to the performance of the Thorlabs RP25.

From Figures 3.15 and 3.16 it can be noted that, with the increase in collection fibers, the spectral integrity is maintained and that the total collected power increases linearly, presenting a linear correlation coefficient of $r^2 = 0.9955$ and a slope of approximately 5.9 mW per fiber.

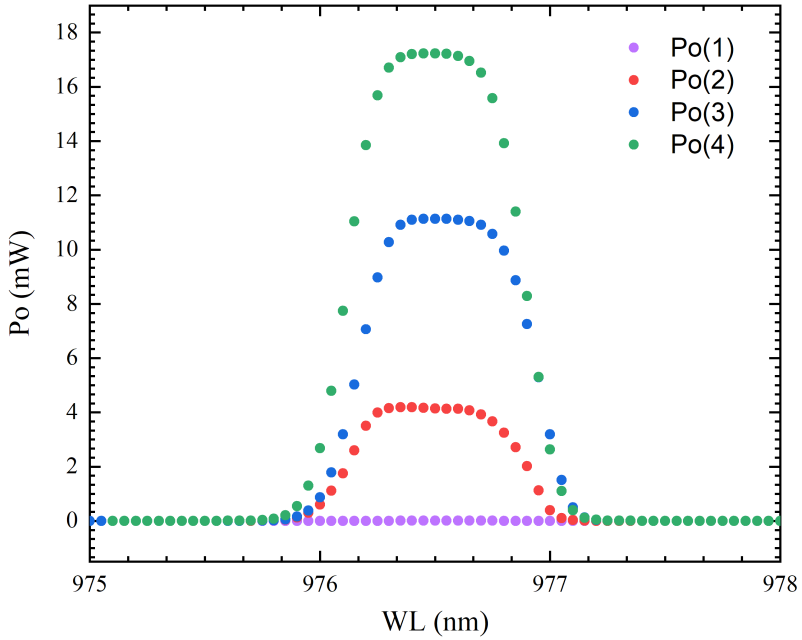

FIGURE 3.15: Laser spectrum evolution for the different numbers of collection fibers.

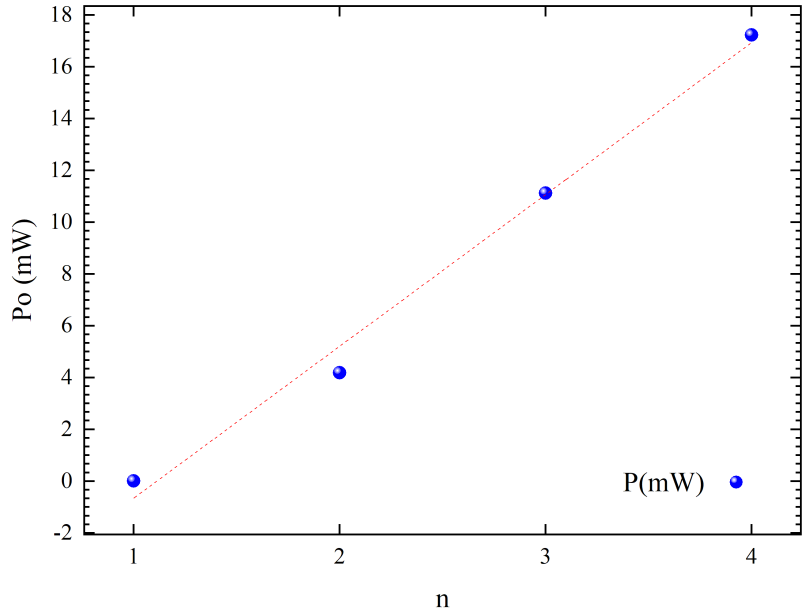

FIGURE 3.16: Evolution of peak power for the different numbers of collection fibers.

3.3.2 Probe tip fabrication

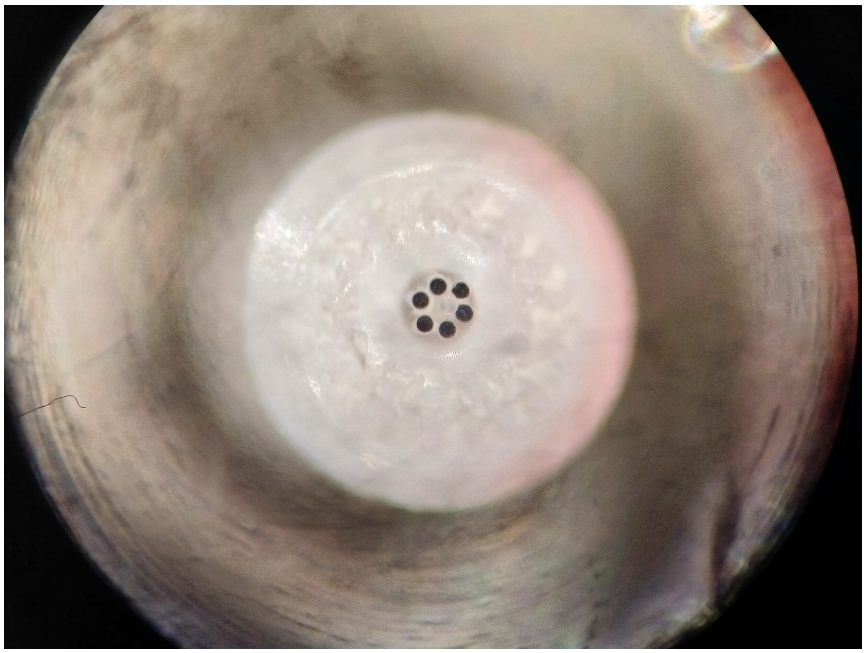

FIGURE 3.17: Photograph of the fabricated probe.

Having studied the emission and collection independently, we were in position to develop a complete probe tip. The chosen design is what is called a six around one, which consists of a single emission fiber, surrounded by six collection fibers, arranged in a close packed configuration. This design was simple and inexpensive to achieve, due to the

fact that, beyond the cleaved fiber tips, there are no additional optics to manufacture or integrate. In order to partially circumvent this limitation and allow for greater flexibility, the probe was built inside the bore of a Thorlabs B30440C connector. This allowed the future connection to a Thorlabs F280FC-980 collimation package which, by itself, would also enable the addition of a lens to focus the beam.

Due to the lack of fabrication manuals and clues, several weeks of surveying literature and trial and error were necessary to arrive at the final solution here described. There amount of HC-PCF available at this stage was insufficient for the construction of a full prototype, therefore, the fiber used for the excitation channel was Thorlabs FG105LCA, the same as the one used for the collection branch. In total four exemplars of this probe design were built during the course of the work for this thesis.

The probe's manufacture begins by unrolling the necessary length of fiber. Approximately seven, 2 m sections are sufficient for our purposes. Next, in order to guarantee the desired geometry, the fibers are passed through the holes of a micro-perforated tube whose capillary pattern corresponds to the desired honeycomb. The first fiber is inserted through the center hole and marked as being the emission channel. Then, the remaining fibers are inserted in the surrounding holes. The next step consists in individually stripping approximately 5 cm from the tip of each of the fibers. Next, to ensure alignment and a clean cleave of the bundle, the fibers are secured in place by means of heat shrink which is inserted in front of the perforated tube and heated until it becomes tight. From here, the bundle is cleaved in a single pass by using a FiTeL No.S323 cleaver. The bundle is then inserted into the bore of the Thorlabs B30440C connector until approximately 1 cm of the front of the bundle exits the outlet of the connector. Super glue (Loctite) is spread into the bundle, close to the tip of the connector. This portion of the bundle is retracted into the bore until approximately 0.5 cm of fiber extends from the connector. Everything is left to dry until the glue hardens, and the fibers remain securely fixed in place inside the bore.

To conclude, the fiber tip must be carefully sanded and polished by performing figure eight movements with the tip placed on 2000 grit sanding paper, for approximately three minutes. Regular stops to observe the tip at the microscope allow the monitoring of the tip's evolution. The same procedure is repeated for 5000 grit sandpaper. After the sanding is completed, the tip is polished with liquid polish (Titanlux) and a microfiber cloth. This allowed buffing the probe until the face of the fibers was completely smooth, providing a good optical interface, flush with the connector's ferrule.

3.3.3 3D Printed Components

For the construction of a complete fiberscope prototype, some components like the stainless-steel sheath and the furcation tubing, were commercially available, however, others had to be custom parts. For the fabrication of these custom pieces, several possibilities were considered, however, due to its accessibility, versatility and speed, 3D printing was the chosen method. The components were first designed in a CAD software (FreeCAD) and then printed in a Zortrax M200 3D printer

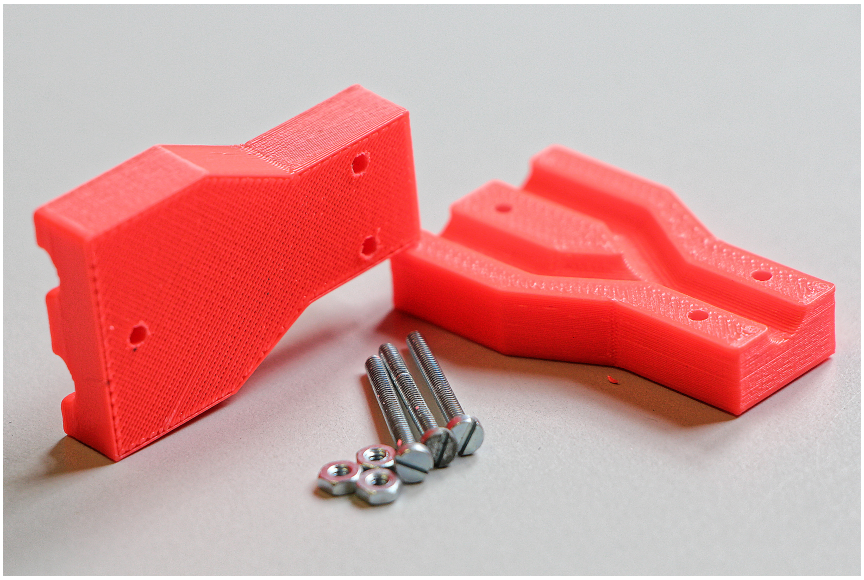

FIGURE 3.18: Photograph of the Y conduit.

The first component to be composed and printed was the Y conduit that joins the emission and collection branch of the fiberscope. As can be seen in Figure 3.18, on the branch side, the part consists of a 25 mm wide section with two inlets, each with a diameter of 5.2 mm, 12 mm apart. The probe side is 15 mm wide and presents a single outlet, also 5.2 mm in diameter. In total, the piece has a length of 40 mm and a height of 15 mm.

To avoid deformation during the deposition process, this connector was sliced in its horizontal plane and printed in two halves, which were then drilled in three points and fixed together by M2 screws and nuts. This also permits easier integration into the fiberscope by allowing the fiber, furcation tubing and stainless-steel sheath to be positioned in place before closing the conduit.

The second component fabricated by this method was actually printed three times. It consisted of a simple tubular interface which was supposed to fix the FC/PC connectors at the end of the three branches. The first attempt at producing this part followed the

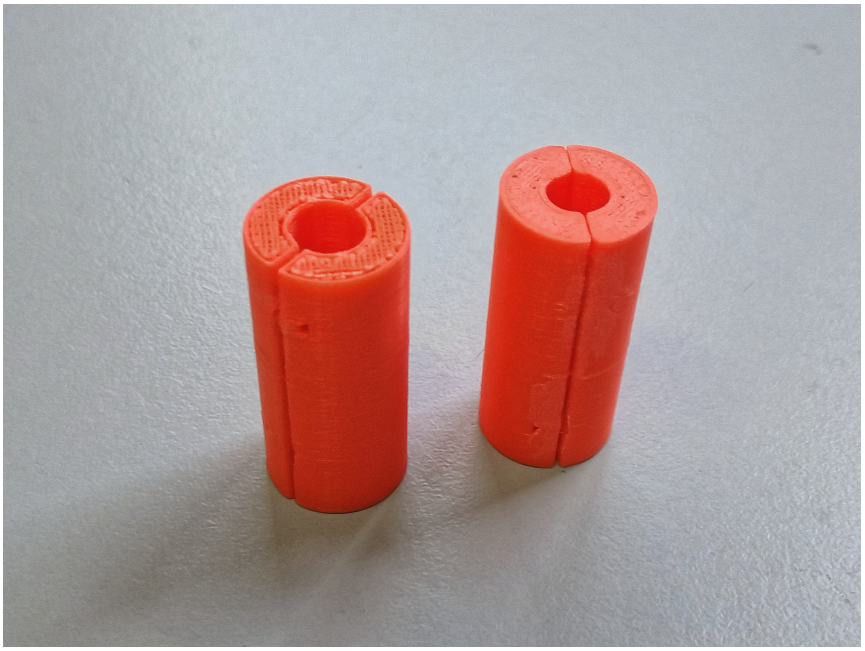

FIGURE 3.19: Photograph of the 3D printed connector interfaces.

same method as described above, however, due to size limitations, it wasn't possible to achieve a bond between the two halves strong enough to hold the sheath in place. In the second attempt, the part was printed in vertical position in a single piece, however, this caused the printing process to include vertical supports inside it, rendering the connector unusable. At a third attempt, the component was printed in horizontal position, however, this caused the inner tube to become slightly deformed and it had to be shaved with a dremel.

In Figure 3.19 a photograph of this component can be seen. It consisted of a 35 mm long cylinder with a 4 mm long waist at 10 mm. Above the waist, the walls of the cylinder were 7.5 mm thick, while bellow they had a thickness of 6.8 mm. At the waist the walls were 8.8 mm. This solution was eventually abandoned in favor of a simpler and more robust interface, achieved with heat shrink and Super Glue.

An additional support for observation of the probe ends was also printed. Please refer to Appendix A for a photograph and the description of this piece.

3.3.4 Filter and Filter Holder Characterization

(A) Photograph of the filter holder.

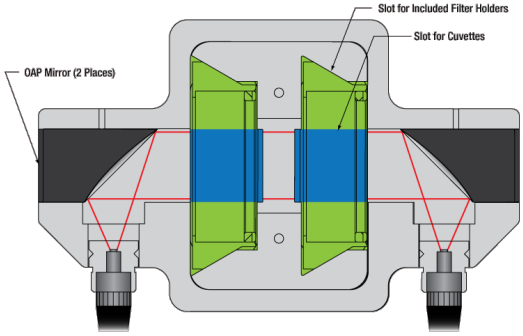

(B) Schematic of the filter holder's insides.

FIGURE 3.20: Photograph and schematic of the filter holder. Adapted from [67].

Due to the silica background Raman signal, inherent to solid core optical fibers, and to the collection of Rayleigh scattering from the sample, filters are among the most important components of an endoscopic system of the class of the one we have been developing. Like mentioned in section 2.2.3 the filters are usually either directly integrated into the design of the probe tip or, they are placed in a section of free space optical path by the use of a dichroic beam splitter. In our case, we opted to resort to a Thorlabs FOFMF filter holder, which made it simple to integrate filters into the collection branch of our system.

Since our excitation wavelength is of 980 nm, this results in our spectra being limited to the wavenumber region above 245.9 cm^{-1} in terms of Raman shift. In Figure 3.20 a photo and a schematic of the filter holder can be seen. Internally, it comprises of two silver coated mirrors which couple light from the input and output connectors, and of a slotted chamber where up to two filters can be inserted into by means of threaded supports. The bandpass filter available was a Thorlabs FELH1000.

FIGURE 3.21: Schematic of the setup assembled for testing the filter and the filter holder.

In order to understand the losses incurred by the integration of this component and to check the performance of the filter, we coupled a broad spectrum source (1500 nm to 1600 nm) and measured the total emitted power with the PM100D OPM. Resorting to the Yokogawa AQ6370 OSA, we also acquired the spectra of the source with, and without, the filter holder or the filter in place, with the purpose of verifying if spectral integrity was maintained. In total, four measurements of power and spectra were made: the broadband source connected directly into the OPM's input; the source connected into the empty filter holder; the same as before but with the filter placed in the first chamber; the same as before but with the filter placed in the second chamber. A schematic of the setup for this experiment can be seen in Figure 3.21.

Configuration	Losses
No filter	−2.992 dB
Filter on the right	−3.025 dB
Filter on the left	−3.052 dB

TABLE 3.2: Powers measured for the different configurations.

The results of the power measurements can be seen in table 3.2. Connecting the filter holder and the filter introduces a power loss of approximately 3 dB which is significant but acceptable. In terms of spectral integrity, by observing the graph shown in Figure 3.22 we conclude that the spectral deformation caused by introduction of the filter holder or the filters is very low, the power difference at each point remaining under 10% to the original spectrum of the source. The additional noise that can be observed is caused by the signal amplification in the OSA itself.

3.3.5 Final Prototype description

Summing together all the work reported in the sections above, we arrive at our final prototype system. It is composed of three main sections: the excitation laser (976 nm), the fiberscope, and the spectrograph. The fiberscope itself consists of the emission and collection branches, connected to the probe branch by the Y conduit described in section 3.3.3 at the center. The branches themselves are constructed by passing the fibers inside Thorlabs FT030-Y furcation tubing, which is then inserted into Thorlabs FT05SS stainless-steel sheath. The probe is of a simple six-around-one design, described in section 3.3.2. It possesses no additional optics and was built inside the bore of a Thorlabs B30440C connector.

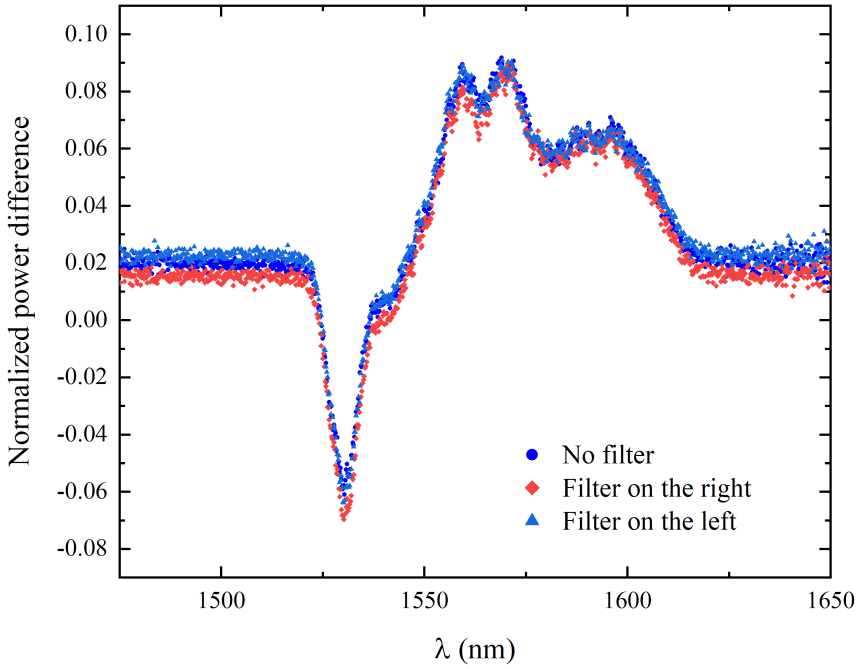

FIGURE 3.22: Graph of the spectra collected directly from the broadband source and the filter holder.

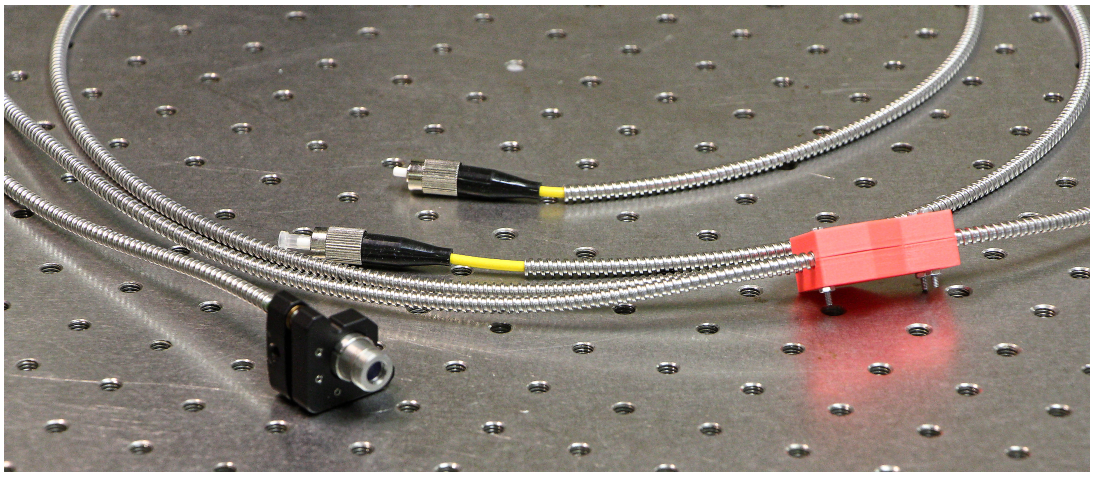

FIGURE 3.23: Photograph of the final prototype. A Thorlabs F280C-980 collimator is connected to the probe as an example of the integration of additional optics.

The collection branch connects to the Thorlabs FOFMF filter holder, characterized in section 3.3.4, containing a Thorlabs bandpass filter, which will then connect to a Thorlabs OSA201C spectrometer. A photograph of the fiberscope can be seen in Figure 3.23 and a schematic of the complete system can be observed in Figure 3.24.

3.3.6 Prototype Characterization

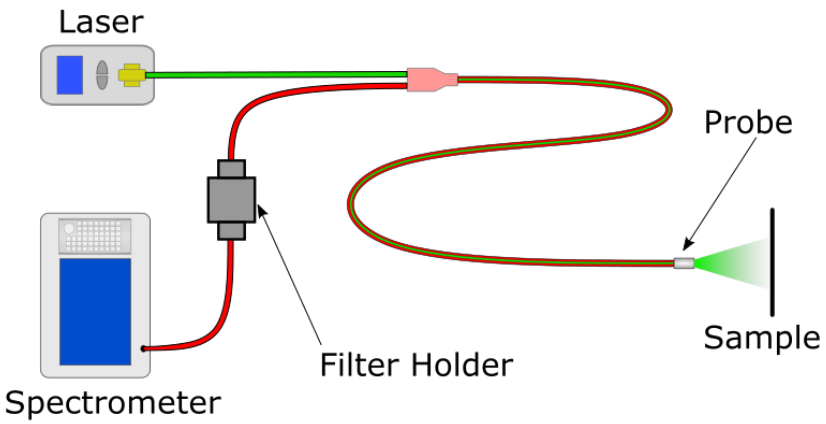

FIGURE 3.24: Schematic of the final fiberscope prototype.

After some trial experiments, it was concluded that due to the λ^{-4} dependency of the Raman signal intensity, a maximum excitation power of 460 mW was insufficient for detection. This prompted the recourse to a BWT 140W Wavelength Stabilized high power laser, with a maximum output of 140 W, operating at 976 nm. A preliminary experiment, without the inclusion of the filter holder, was performed with this laser, which consisted in the illumination of a thin film of Silicon, deposited over a microscope slide and of a Paracetamol pill. The pill was divided in two and, for each of the resulting halves, the probe tip was aligned with the exposed internal face.

The excitation current of the laser was set to 0.69 mA, which resulted in 800 mW of laser power at the sample. The collected spectra were measured by taking 50 acquisitions with the Thorlabs OSA201C and calculating their average.

The superposition of the spectrum acquired in the preliminary measurement with a reference example can be observed in Figure 3.25. The general signal intensity was quite low, with shot-noise being very prevalent despite the considerable number of acquisitions. Denoising, smoothing and baseline removal processes were necessary in order to make the comparison between spectra more immediate. It should be noted that the line of the spectrum acquired with the prototype crosses the horizontal axis as a consequence of the baseline subtraction.

The expected Raman shift for the principal peak of Silicon is 521.26 cm^{-1}. As can be observed here the spectrum obtained is different from the one expected, presenting several additional features. For the Paracetamol sample, the prototype acquired an identical

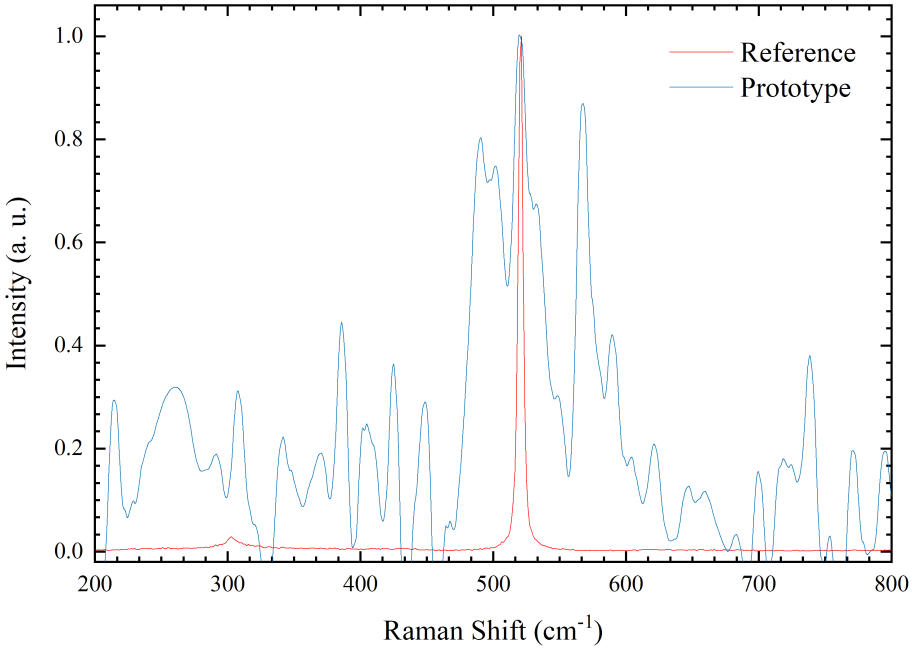

FIGURE 3.25: Graph of the preliminary Silicon signal, superimposed with a reference spectrum.

spectrum, therefore, this signal must result from one of the system's components, drowning the Raman spectrum of the sample. To achieve validation of the prototype, further investigation into this matter is necessary.

3.4 Closing remarks

In this chapter we got to better understand the advantages that HC-PCF has over SMF in terms of light guiding and delivery, showing that it presents much lower losses and that it is insensitive to curvature. The beam output by a cleaved tip of this fiber was characterized and compared to the one emitted by an RP25 bundle from Thorlabs, tracing their longitudinal, transverse, and angular profile. From that knowledge and form studying several collection configurations, we were in position of developing and fabricating a simple and inexpensive probe tip and of assembling a complete fiberscope system. As previously mentioned, filters are essential for optimal performance, therefore, a Thorlabs FOFMF filter holder and a FELH1000 filter were also integrated and characterized. Having the complete system, preliminary measurements of Silicon and Paracetamol samples were acquired. Despite the fact that validation of our prototype will have to be deferred to future work, the knowledge and experience gained with the work reported in this chapter

are important know-how, and show that achieving a complete, functioning fiberscope for Raman endoscopy might be possible in the near future.

Chapter 4

Raman Spectroscopy

This chapter reports the collection of spectra with a confocal Raman spectrometer from Renishaw. These measurements, along with providing hands-on experience with operation of state-of-the-art equipment, they also brought additional education on the technique and relevant insights for the successful implementation of a fiberscope system.

As demonstrated in section 2.3, biomedical and clinical fields are among the most relevant in terms of application of this technology. This, combined previous experience in the measurement of Raman spectra of different pharmaceutical and biological samples [69, 70], led to the choice of Ben-u-Ron pills, a common medicine whose active substance is Paracetamol, as samples. The results obtained with this spectrometer returned reference spectra that would help validate the assembled prototype.

4.1 Instrumentation

The spectrometer available at the institute (Figure 4.1) consists of a Renishaw InVia™ Qontor®, which provides state of the art Raman spectra acquisition. It is based on a confocal system, and resorts to a Charge Coupled Device (CCD) for detection. This CCD is composed of 1024x256 pixels and is kept at a constant temperature of 203.15 K ($-70\,^{\circ}$C) by Peltier effect, presenting high sensitivity in the 200 nm to 1064 nm range. This system grants a spectral range from 100 cm^{-1} to 4000 cm^{-1}, and a spectral resolution of over 3 cm^{-1} for each of the three excitation wavelengths available: 532 nm, 633 nm and 785 nm. The spectrometer also includes an integrated microscope, allowing real-time observation of the samples, which are prepared in a slide and placed in the stage under the objective.

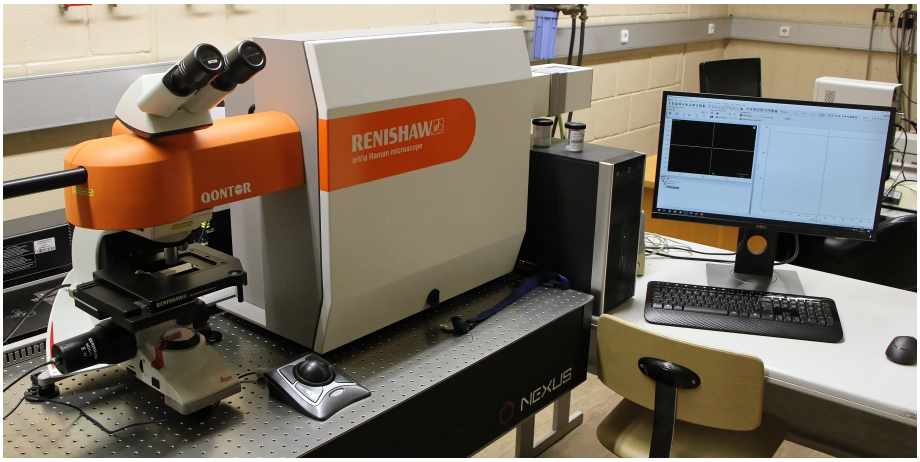

FIGURE 4.1: Photograph of the Renishaw InVia™ system used for the collection of spectra.

Before proceeding with the measurement of the Raman spectrum of the desired sample, it is necessary to perform a calibration of the instrument, achieved by analyzing a sample of a thin film of Silicon, deposited on the surface of a microscope slide. Silicon is ideal for this purpose because it presents a single, very well defined peak at 521 cm^{-1} and the resulting spectrum can be seen in red in Figure 3.25. As mentioned in section 3.3.6, this sample was also measured in the preliminary experiments performed with the prototype.

4.2 Paracetamol

For the measurements made at the Renishaw spectrometer, the pills were reduced to powder before being placed into the spectrometer. In total, eight spectra were acquired in different locations of the sample and all the measurements were performed with an excitation wavelength of 633 nm, at 50% of the total available power, and for a total of 30 s of exposition time. At this excitation wavelength some fluorescence is expected. It manifests itself as some additional noise and a wideband baseline signal that needs to be removed in order to isolate the desired Raman spectra. The removal of this component was achieved by importing the data into a specialized software for graphical data analysis. The process itself consists in the selection of several points along the spectra that are then used as nodes of a numerical BSpline algorithm. For each unit of Raman shift, this algorithm returns a value of the spline that is then subtracted to the intensity value, resulting in spectra with a mostly flat baseline. An example of a complete spectrum of Paracetamol

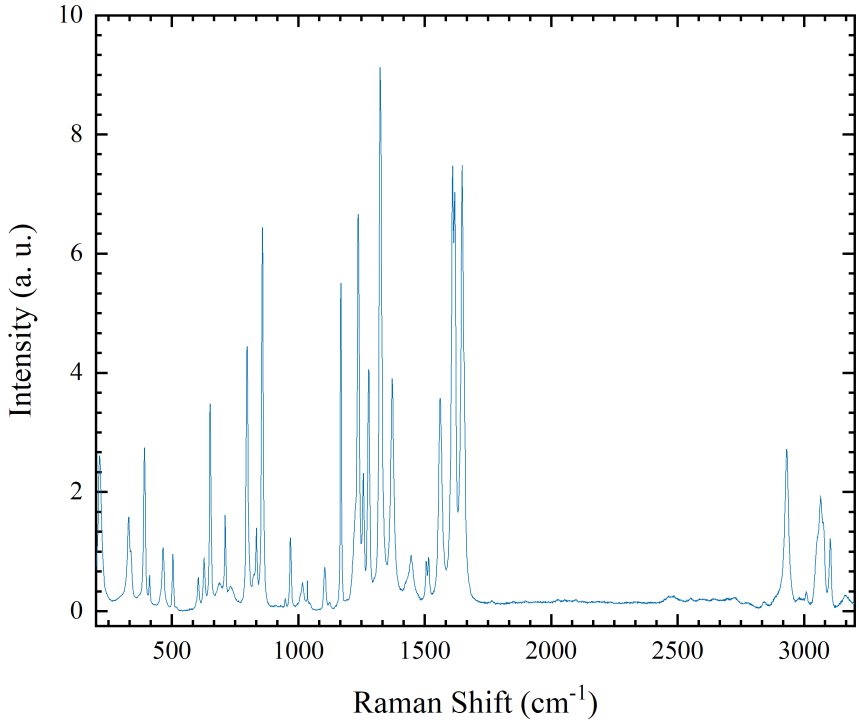

FIGURE 4.2: Graph of the spectrum acquired by the Renishaw spectrometer for Paracetamol powder.

after this process as applied can be observed in Figure 4.2. A table with the centers of the peaks can be seen in Table C.1 from Appendix C.

4.3 Closing remarks

In this chapter, we described a top-of-the-line confocal spectrometer and the procedures taken for the acquisition and analysis of spectra from a Silicon thin film and from Paracetamol powder. These spectra had the purpose of providing a reference that would allow the validation of the fiberscope system described in the previous chapter. However, important experimental differences and the very preliminary state of the prototype, make the comparison impractical.

Chapter 5

Conclusions and Future Work

This thesis reports of the first steps in the development of a fiberscope for collection of Raman spectra. Going from very initial measurements related to the light guiding characteristics of SMF and HC-PCF, to preliminary experiments with a complete prototype, it provided many valuable learning experiences. It also illuminates the many challenges that the successful development of such technology entails, demonstrating that these systems are beyond trivial bundles of fibers.

In more detail, the first step taken consisted in obtaining some sensibility about how HC-PCF compares to SMF in terms of transmission losses and of sensitivity to curvature. From the power sweep of the excitation current of an input laser, it was shown that across the range of measured powers, the HC-PCF presents an output two times greater than what the SMF provides, the slope being over three times greater. In terms of curvature sensitivity, the HC-PCF demonstrated great performance by not having its output power reduced, even for very small loops. These two results show that, beyond not suffering from an intrinsic Raman background, the HC-PCF possesses additional advantages over SMF for the delivery of the excitation laser.

With this in mind, the beam output by a cleaved tip of HC-PCF was characterized by measuring its longitudinal, transverse, and angular profiles. It was shown that power decays exponentially with distance from the fiber tip, with a constant of 5.41 mm, and that the transverse and angular profiles are both Gaussian, the transverse profile having a FWHM of approximately 9.9 mm.

After understanding the emission characteristics of HC-PCF, several configurations with increasing numbers of collection fibers were studied in terms of their light collection

capability. It was demonstrated that in the case of suboptimal light coupling, a configuration built in-house had potential to match a commercial solution and that, in the case of optimal light coupling, its performance would be surpassed. It was also shown that spectral integrity was maintained with the increase of the number of collection fibers and that peak intensity increases linearly.

These encouraging results led to the design of a simple six-around-one probe tip whose fabrication method is described, and to the construction of a complete fiberscope prototype from custom and commercially available parts. Filters were introduced by means of a FOFMF filter holder integrated into the collection channel, which was characterized in terms of losses and spectral integrity. The final prototype is described, and preliminary experiments are reported.

As a means of acquiring additional know-how on Raman spectroscopy as a whole and obtaining reference spectra for the validation of the fiberscope, the contact with a state-of-the-art Renishaw spectrometer is reported. In particular, spectra from a Silicon thin film and from Paracetamol powder were acquired.

Despite the fact that achieving validation of the prototype will have to be deferred to future work, the results are promising, and this work represents an important stepping stone, providing substantial information about the fundamentals, the difficulties, and challenges involved in the development of such a system. In order to achieve a fully functioning system, capable of collecting correct and verifiable spectra, the next steps involve:

- Further development of the probe tip, produce probes with HC-PCF.
- The introduction of more advanced probe designs and fabrication techniques.
- Optimization of the current system by a greater understanding of how the different components contribute to the overall performance.
- Achieve validation by comparison with reference spectra.
- An attempt at the collection of spectra from other both solid as well as liquid samples.

Appendix A

3D printed mirror support

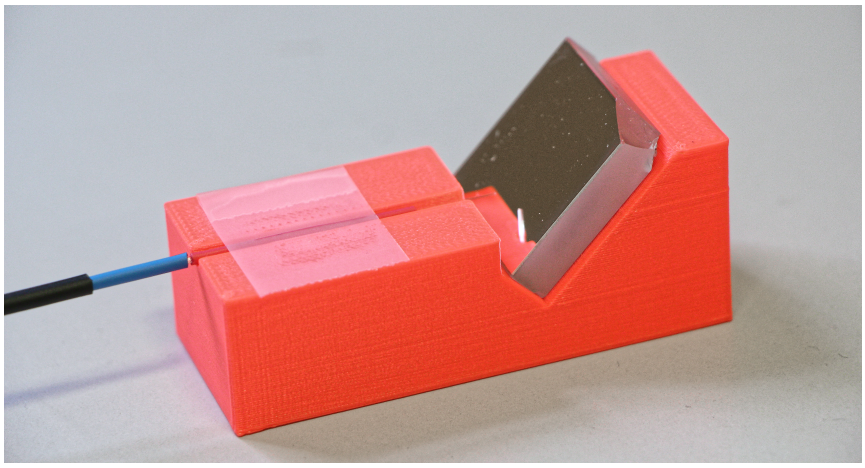

FIGURE A.1: Photograph of the mirror support.

In order to more easily inspect and photograph the front face of the probe tips, a support for a mirror was printed. A photograph of this piece can be seen in Figure A.1. This support was printed in a single piece, however, it is better described as two separate sections. The first section is an elevated platform with a narrow slit, 3 mm in diameter, which supports the piece to be observed, while the second section consists of a 45° ramp which supports the mirror. The part is 65 mm long, has a height of 25 mm and a thickness of 26 mm.

With this support, it was simple to inspect the evolution of the probe's fabrication process by placing them under a microscope.

Appendix B

Fiber Specifications

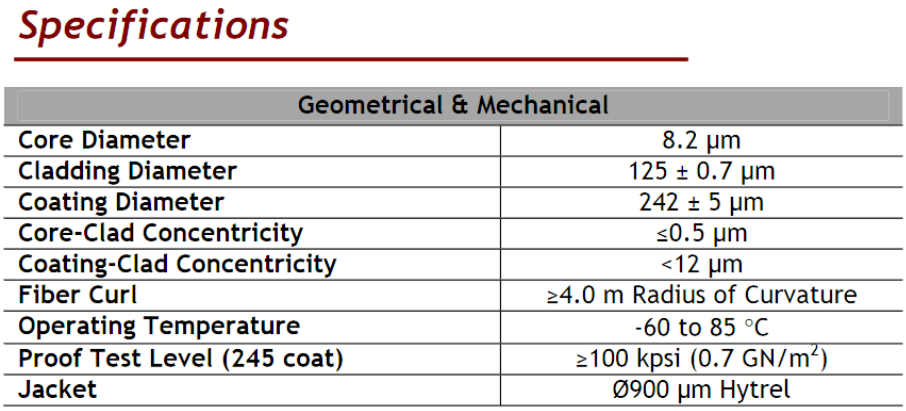

Specifications

Geometrical & Mechanical	
Core Diameter	8.2 µm
Cladding Diameter	125 ± 0.7 µm
Coating Diameter	242 ± 5 µm
Core-Clad Concentricity	≤0.5 µm
Coating-Clad Concentricity	<12 µm
Fiber Curl	≥4.0 m Radius of Curvature
Operating Temperature	-60 to 85 °C
Proof Test Level (245 coat)	≥100 kpsi (0.7 GN/m^2)
Jacket	Ø900 µm Hytrel

FIGURE B.1: Specifications of the Thorlabs SMF28 used. Adapted from [67].

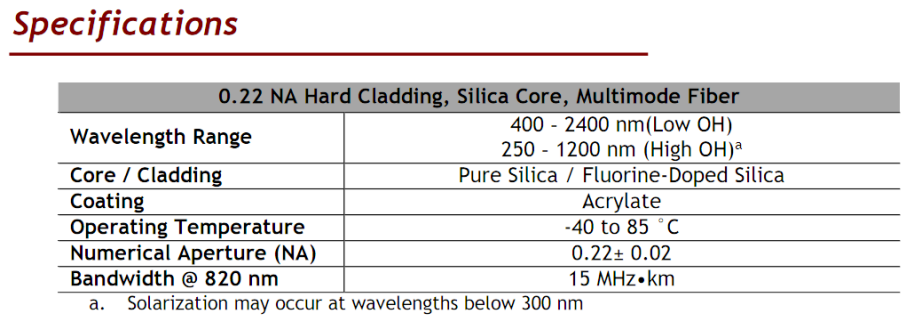

Specifications

0.22 NA Hard Cladding, Silica Core, Multimode Fiber	
Wavelength Range	400 - 2400 nm(Low OH) 250 - 1200 nm (High OH)[a]
Core / Cladding	Pure Silica / Fluorine-Doped Silica
Coating	Acrylate
Operating Temperature	-40 to 85 °C
Numerical Aperture (NA)	0.22± 0.02
Bandwidth @ 820 nm	15 MHz•km

a. Solarization may occur at wavelengths below 300 nm

FIGURE B.2: Specifications of the Thorlabs MMF FG105LCA used. Adapted from [67].

Physical properties	
Core diameter*	10 µm ± 1 µm
Pitch	2.75 µm
Air filling fraction PBG region	› 90%
Diameter of holey region	50 µm
Cladding diameter	123 µm ± 5 µm
Coating diameter (single layer acrylate)	220 µm ± 50 µm

FIGURE B.3: Specifications of the Thorlabs HC-1060 used. Adapted from [67].

Item #	Fiber Configurations
RP24	
RP25	

Item #[a]	Hydroxyl Content	Wavelength Range	Fiber Item #	Light Source Leg	Sample Leg	Spectrometer Leg	Fiber Core Diameter	Fiber Cladding Diameter	NA	Minimum Bend Radius		Fiber Attenuation Plot
										Short Term[e]	Long Term[f]	
RP24	High OH	250 - 1200 nm[b]	FG200UEA	SMA Connector, Single Fiber	Ø1/4" Probe[c]	SMA Connector, Linear Bundle	200 µm ± 2%	220 ± 2 µm	0.22[d]	19 mm	53 mm	
RP25	Low OH	400 - 2400 nm	FG200LEA									

FIGURE B.4: Specifications of the Thorlabs RP25 fiber bundle. Adapted from [67].

Appendix C

Paracetamol spectrum peak centers

Peak Centers (cm^{-1})	Peak Centers (cm^{-1})
108.938477	1630.132813
115.499023	1647.647461
127.292969	2892.282227
150.818359	2897.168945
215.743164	2903.676758
328.515625	2906.115234
391.754883	2908.551758
464.366211	2913.421875
652.150391	2919.097656
709.962891	2923.148438
798.085938	2933.663086
858.118164	2944.960938
969.599609	3043.888672
1103.964844	3046.256836
1167.839844	3050.990234
1236.571289	3056.505859
1257.479492	3062.015625
1279.411133	3069.875977
1323.037109	3073.800781
1371.742188	3076.938477
1560.589844	3081.640625
1610.496094	3085.556641
1618.772461	3101.18457

TABLE C.1: Raman shifts of the centers of the peaks found for the Paracetamol powder, acquired with the Renishaw spectrometer.

Bibliography

[1] G. R. Trott and T. E. Furtak, "Angular resolved Raman scattering using fiber optic probes," *Review of Scientific Instruments*, vol. 51, no. 11, pp. 1493–1496, Nov. 1980. [Online]. Available: http://aip.scitation.org/doi/10.1063/1.1136110 [Cited on pages xiii, 5, and 6.]

[2] H. H. Eysel, "Ramanstreuung polykristalliner substanzen: aufnahme mit hilfe faseloptischer querschnittswandler," *Spectrochimica Acta Part A: Molecular Spectroscopy*, vol. 27, no. 1, pp. 173–177, Jan. 1971. [Online]. Available: https://www.sciencedirect.com/science/article/pii/058485397180020X [Cited on page 5.]

[3] A. Eckbreth, "CARS thermometry in practical combustors," *Combustion and Flame*, vol. 39, no. 2, pp. 133–147, Oct. 1980. [Online]. Available: https://linkinghub.elsevier.com/retrieve/pii/0010218080900139 [Cited on page 5.]

[4] R. L. McCreery, M. Fleischmann, and P. Hendra, "Fiber optic probe for remote Raman spectrometry," *Analytical Chemistry*, vol. 55, no. 1, pp. 146–148, Jan. 1983. [Online]. Available: https://pubs.acs.org/doi/abs/10.1021/ac00252a039 [Cited on page 6.]

[5] J. I. Peterson, R. V. Fitzgerald, and D. K. Buckhold, "Fiber-optic probe for in vivo measurement of oxygen partial pressure," *Analytical Chemistry*, vol. 56, no. 1, pp. 62–67, Jan. 1984. [Online]. Available: https://pubs.acs.org/doi/abs/10.1021/ac00265a017 [Cited on page 6.]

[6] S. D. Schwab and R. L. McCreery, "Versatile, efficient Raman sampling with fiber optics," *Analytical Chemistry*, vol. 56, no. 12, pp. 2199–2204, Oct. 1984. [Online]. Available: https://pubs.acs.org/doi/abs/10.1021/ac00276a049

[7] ——, "Remote, Long-Pathlength Cell for High-Sensitivity Raman Spectroscopy," *Applied Spectroscopy*, vol. 41, no. 1, pp. 126–130, Jan. 1987. [Online]. Available: http://journals.sagepub.com/doi/10.1366/0003702874868089

[8] D. D. Archibald, L. T. Lin, and D. E. Honigs, "Raman Spectroscopy over Optical Fibers with the Use of a Near-IR FT Spectrometer," *Applied Spectroscopy*, vol. 42, no. 8, pp. 1558–1563, Nov. 1988. [Online]. Available: http://journals.sagepub.com/doi/10.1366/0003702884429643

[9] E. N. Lewis, V. F. Kalasinsky, and I. W. Levin, "Near-infrared Fourier-transform Raman spectroscopy using fiber-optic assemblies," *Analytical Chemistry*, vol. 60, no. 24, pp. 2658–2661, Dec. 1988. [Online]. Available: https://pubs.acs.org/doi/abs/10.1021/ac00175a002 [Cited on page 6.]

[10] P. Plaza, N. Q. Dao, M. Jouan, H. Fevrier, and H. Saisse, "Simulation et optimisation des capteurs à fibres optiques adjacentes," *Applied Optics*, vol. 25, no. 19, p. 3448, Oct. 1986. [Online]. Available: https://www.osapublishing.org/abstract.cfm?URI=ao-25-19-3448 [Cited on page 6.]

[11] P. J. Hendra, G. Ellis, and D. J. Cutler, "Use of optical fibres in Raman spectroscopy," p. 6, 1988. [Cited on page 6.]

[12] C. D. Allred and R. L. McCreery, "Near-Infrared Raman Spectroscopy of Liquids and Solids with a Fiber-Optic Sampler, Diode Laser, and CCD Detector," *Applied Spectroscopy*, vol. 44, no. 7, pp. 1229–1231, Aug. 1990. [Online]. Available: http://journals.sagepub.com/doi/10.1366/0003702904086498 [Cited on page 7.]

[13] C. D. Newman, G. G. Bret, and R. L. McCreery, "Fiber-Optic Sampling Combined with an Imaging Spectrograph for Routine Raman Spectroscopy," *Applied Spectroscopy*, vol. 46, no. 2, pp. 262–265, Feb. 1992. [Online]. Available: http://journals.sagepub.com/doi/10.1366/0003702924125447 [Cited on page 7.]

[14] M. L. Myrick, S. M. Angel, and R. Desiderio, "Comparison of some fiber optic configurations for measurement of luminescence and Raman scattering," *Applied Optics*, vol. 29, no. 9, p. 1333, Mar. 1990. [Online]. Available: https://www.osapublishing.org/abstract.cfm?URI=ao-29-9-1333 [Cited on page 7.]

[15] M. L. Myrick and S. M. Angel, "Elimination of Background in Fiber-Optic Raman Measurements," *Applied Spectroscopy*, vol. 44, no. 4, pp. 565–570, May 1990. [Online]. Available: http://journals.sagepub.com/doi/10.1366/0003702904087235 [Cited on page 7.]

[16] B. Yang and M. D. Morris, "Disposable Protective Sheath for the Fiber-Optic Raman Probe," *Applied Spectroscopy*, vol. 45, no. 3, pp. 512–513, Mar. 1991. [Online]. Available: http://journals.sagepub.com/doi/10.1366/0003702914337236 [Cited on page 7.]

[17] C. Kong Chong, C. Shen, Y. Fong, J. Zhu, F.-X. Yan, S. Brush, C. K. Mann, and T. J. Vickers, "Raman spectroscopy with a fiber-optic probe," *Vibrational Spectroscopy*, vol. 3, no. 1, pp. 35–45, Mar. 1992. [Online]. Available: https://linkinghub.elsevier.com/retrieve/pii/092420319285022S

[18] J. Barbillat, P. Dhamelincourt, M. Delhaye, and E. Da Silva, "Raman confocal microprobing, imaging and fibre-optic remote sensing: A further step in molecular analysis," *Journal of Raman Spectroscopy*, vol. 25, no. 1, pp. 3–11, Jan. 1994. [Online]. Available: https://onlinelibrary.wiley.com/doi/10.1002/jrs.1250250103

[19] M. L. Myrick, J. Kolis, E. Parsons, K. Chike, M. Lovelace, W. Scrivens, R. Holliday, and M. Williams, "In situ fiber-optic Raman spectroscopy of organic chemistry in a supercritical water reactor," *Journal of Raman Spectroscopy*, vol. 25, no. 1, pp. 59–65, Jan. 1994. [Online]. Available: https://onlinelibrary.wiley.com/doi/10.1002/jrs.1250250109

[20] J. Ma and Y.-S. Li, "Optical-Fiber Raman Probe with Low Background Interference by Spatial Optimization," *Applied Spectroscopy*, vol. 48, no. 12, pp. 1529–1531, Dec. 1994. [Online]. Available: http://journals.sagepub.com/doi/10.1366/0003702944027831 [Cited on page 7.]

[21] T. F. Cooney, H. T. Skinner, and S. M. Angel, "Comparative Study of Some Fiber-Optic Remote Raman Probe Designs. Part I: Model for Liquids and Transparent Solids," *Applied Spectroscopy*, vol. 50, no. 7, pp. 836–848, Jul. 1996. [Online]. Available: http://journals.sagepub.com/doi/10.1366/0003702963905592 [Cited on page 7.]

[22] ——, "Comparative Study of Some Fiber-Optic Remote Raman Probe Designs. Part II: Tests of Single-Fiber, Lensed, and Flat- and Bevel-Tip Multi-Fiber Probes,"

Applied Spectroscopy, vol. 50, no. 7, pp. 849–860, Jul. 1996. [Online]. Available: http://journals.sagepub.com/doi/10.1366/0003702963905574 [Cited on page 7.]

[23] I. R. Lewis and P. R. Griffiths, "Raman Spectrometry with Fiber-Optic Sampling," *Applied Spectroscopy*, vol. 50, no. 10, pp. 12A–30A, Oct. 1996. [Online]. Available: http://journals.sagepub.com/doi/10.1366/0003702963904908 [Cited on page 7.]

[24] J. Ma and Y.-S. Li, "Fiber Raman background study and its application in setting up optical fiber Raman probes," *Applied Optics*, vol. 35, no. 15, p. 2527, May 1996. [Online]. Available: https://www.osapublishing.org/abstract.cfm?URI=ao-35-15-2527 [Cited on page 7.]

[25] J. T. Motz, M. Hunter, L. H. Galindo, J. A. Gardecki, J. R. Kramer, R. R. Dasari, and M. S. Feld, "Optical fiber probe for biomedical Raman spectroscopy," p. 13, 2004. [Cited on pages xiii, 7, and 8.]

[26] K. P. J. Williams, "Remote sampling using a fibre-optic probe in fourier transform Raman spectroscopy," *Journal of Raman Spectroscopy*, vol. 21, no. 2, pp. 147–151, Aug. 1996. [Online]. Available: https://onlinelibrary.wiley.com/doi/10.1002/jrs.1250210213 [Cited on page 8.]

[27] G. Zhang, S. G. Demos, and R. R. Alfano, "Raman spectra of biomedical samples using optical fiber probes," in *Biomedical Sensing, Imaging, and Tracking Technologies II*, vol. 2976. International Society for Optics and Photonics, Jun. 1997, pp. 2–9. [Online]. Available: https://www.spiedigitallibrary.org/conference-proceedings-of-spie/2976/0000/Raman-spectra-of-biomedical-samples-using-optical-fiber-probes/10.1117/12.275522.short

[28] M. G. Shim and B. C. Wilson, "Development of an In Vivo Raman Spectroscopic System for Diagnostic Applications," *Journal of Raman Spectroscopy*, vol. 28, p. 12, 1997.

[29] Y. Komachi, H. Sato, Y. Matsuura, M. Miyagi, and H. Tashiro, "Raman probe using a single hollow waveguide," p. 3, 2005. [Cited on page 8.]

[30] Y. Komachi, T. Katagiri, H. Sato, and H. Tashiro, "Improvement and analysis of a micro Raman probe," p. 14, 2008. [Cited on page 8.]

[31] A. Mahadevan-Jansen, M. F. Mitchell, N. Ramanujam, U. Utzinger, and R. Richards-Kortum, "Development of a Fiber Optic Probe to Measure NIR Raman Spectra of Cervical Tissue In Vivo," *Photochemistry and Photobiology*, vol. 68, no. 3, pp. 427–431, 1998, _eprint: https://onlinelibrary.wiley.com/doi/pdf/10.1111/j.1751-1097.1998.tb09703.x. [Online]. Available: https://onlinelibrary.wiley.com/doi/abs/10.1111/j.1751-1097.1998.tb09703.x [Cited on page 8.]

[32] U. Utzinger and R. R. Richards-Kortum, "Fiber optic probes for biomedical optical spectroscopy," *Journal of Biomedical Optics*, vol. 8, no. 1, pp. 121–147, Jan. 2003, publisher: International Society for Optics and Photonics. [Online]. Available: https://www.spiedigitallibrary.org/journals/journal-of-biomedical-optics/volume-8/issue-1/0000/Fiber-optic-probes-for-biomedical-optical-spectroscopy/10.1117/1.1528207.short [Cited on pages 8 and 15.]

[33] R. F. Cregan, B. J. Mangan, J. C. Knight, T. A. Birks, P. S. J. Russell, P. J. Roberts, and D. C. Allan, "Single-Mode Photonic Band Gap Guidance of Light in Air," *Science*, vol. 285, no. 5433, pp. 1537–1539, Sep. 1999. [Online]. Available: https://www.science.org/doi/10.1126/science.285.5433.1537 [Cited on pages 8 and 12.]

[34] S. O. Konorov, A. M. Zheltikov, and M. Scalora, "Photonic-crystal fiber as a multifunctional optical sensor and sample collector," p. 6, 2005. [Cited on page 8.]

[35] A. Argyros, M. A. van Eijkelenborg, M. C. J. Large, and I. M. Bassett, "Hollow-core microstructured polymer optical fiber," p. 3, 2006.

[36] S. O. Konorov, C. J. Addison, H. G. Schulze, and R. F. B. Turner, "Hollow-core photonic crystal fiber-optic probes for Raman spectroscopy," p. 3, 2006.

[37] A. Khetani, J. Riordon, V. Tiwari, A. Momenpour, M. Godin, and H. Anis, "Hollow core photonic crystal fiber as a reusable Raman biosensor," p. 11, 2013. [Cited on page 12.]

[38] S. Inoue, T. Katagiri, and Y. Matsuura, "Fiber optic direct Raman imaging system based on a hollow-core fiber bundle," in *Optical Fibers and Sensors for Medical Diagnostics and Treatment Applications XV*, vol. 9317. International Society for Optics and Photonics, Mar. 2015, p. 93170V. [Online]. Available: https://www.spiedigitallibrary.org/conference-proceedings-of-spie/9317/93170V/Fiber-

optic-direct-Raman-imaging-system-based-on-a-hollow/10.1117/12.2078662.short [Cited on page 8.]

[39] C. A. Ross, D. G. MacLachlan, B. J. E. Smith, R. J. Beck, J. D. Shephard, N. Weston, and R. R. Thomson, "A Miniature Fibre-Optic Raman Probe Fabricated by Ultrafast Laser-Assisted Etching," *Micromachines*, vol. 11, no. 2, Feb. 2020. [Online]. Available: https://europepmc.org/articles/PMC7074630 [Cited on pages xiii and 8.]

[40] O. R. Šćepanović, Z. Volynskaya, C.-R. Kong, L. H. Galindo, R. R. Dasari, and M. S. Feld, "A multimodal spectroscopy system for real-time disease diagnosis," *Review of Scientific Instruments*, vol. 80, no. 4, p. 043103, Apr. 2009. [Online]. Available: http://aip.scitation.org/doi/10.1063/1.3117832 [Cited on page 8.]

[41] M. Sharma, E. Marple, J. Reichenberg, and J. W. Tunnell, "Design and characterization of a novel multimodal fiber-optic probe and spectroscopy system for skin cancer applications," *The Review of Scientific Instruments*, vol. 85, no. 8, p. 083101, Aug. 2014. [Online]. Available: https://www.ncbi.nlm.nih.gov/pmc/articles/PMC4137875/

[42] X. Chen, X. Xu, D. T. McCormick, K. Wong, and S. T. C. Wong, "Multimodal nonlinear endo-microscopy probe design for high resolution, label-free intraoperative imaging," p. 11, 2015.

[43] E. Garai, S. Sensarn, C. L. Zavaleta, N. O. Loewke, S. Rogalla, M. J. Mandella, S. A. Felt, S. Friedland, J. T. C. Liu, S. S. Gambhir, and C. H. Contag, "A Real-Time Clinical Endoscopic System for Intraluminal, Multiplexed Imaging of Surface-Enhanced Raman Scattering Nanoparticles," *PLOS ONE*, p. 16, 2015.

[44] A. Lombardini, V. Mytskaniuk, S. Sivankutty, E. R. Andresen, X. Chen, J. Wenger, M. Fabert, N. Joly, F. Louradour, A. Kudlinski, and H. Rigneault, "High-resolution multimodal flexible coherent Raman endoscope," *Light: Science & Applications*, vol. 7, no. 1, p. 10, May 2018, bandiera_abtest: a Cc_license_type: cc_by Cg_type: Nature Research Journals Number: 1 Primary_atype: Research Publisher: Nature Publishing Group. [Online]. Available: https://www.nature.com/articles/s41377-018-0003-3 [Cited on page 8.]

[45] S. Yerolatsitis, F. Yu, S. McAughtrie, M. G. Tanner, H. Fleming, J. M. Stone, C. J. Campbell, T. A. Birks, and J. C. Knight, "Ultra-low background Raman sensing using a negative-curvature fibre and no distal optics," *Journal of Biophotonics*, vol. 12, no. 3, p. e201800239, 2019, _eprint: https://onlinelibrary.wiley.com/doi/pdf/10.1002/jbio.201800239. [Online]. Available: https://onlinelibrary.wiley.com/doi/abs/10.1002/jbio.201800239 [Cited on page 8.]

[46] C. Kong, C. Pilger, H. Hachmeister, X. Wei, T. H. Cheung, C. S. W. Lai, N. P. Lee, K. K. Tsia, K. K. Y. Wong, and T. Huser, "High-contrast, fast chemical imaging by coherent Raman scattering using a self-synchronized two-colour fibre laser," *Light: Science & Applications*, vol. 9, no. 1, p. 25, Feb. 2020, bandiera_abtest: a Cc_license_type: cc_by Cg_type: Nature Research Journals Number: 1 Primary_atype: Research Publisher: Nature Publishing Group Subject_term: Confocal microscopy;Fibre lasers Subject_term_id: confocal-microscopy;fibre-lasers. [Online]. Available: https://www.nature.com/articles/s41377-020-0259-2 [Cited on page 8.]

[47] I. E. Iping Petterson, J. C. C. Day, L. M. Fullwood, B. Gardner, and N. Stone, "Characterisation of a fibre optic Raman probe within a hypodermic needle," *Analytical and Bioanalytical Chemistry*, vol. 407, no. 27, pp. 8311–8320, Nov. 2015. [Online]. Available: http://link.springer.com/10.1007/s00216-015-9021-7 [Cited on page 8.]

[48] J. R. Ferraro, K. Nakamoto, and C. W. Brown, *Introductory Raman Spectroscopy*. Academic Press, Jan. 2003. [Cited on page 11.]

[49] D. A. Long, *The Raman Effect: A Unified Treatment of the Theory of Raman Scattering by Molecules*. John Wiley & Sons, Ltd, Apr. 2002. [Cited on page 11.]

[50] D. Pristinski and H. Du, "Solid-core photonic crystal fiber as a Raman spectroscopy platform with a silica core as an internal reference," p. 3, 2006. [Cited on page 12.]

[51] M. Balu, G. Liu, Z. Chen, and E. O. Potma, "Fiber delivered probe for efficient CARS imaging of tissues," p. 9, 2010.

[52] S. Brustlein, P. Berto, R. Hostein, P. Ferrand, D. Marguet, A. Muir, and J. Knight, "Double-clad hollow core photonic crystal fiber for coherent Raman endoscope," p. 7, 2011.

[53] C. Raml, X. He, M. Han, D. R. Alexander, and Y. Lu, "Raman spectroscopy based on a single-crystal sapphire fiber," *Optics Letters*, vol. 36, no. 7, p. 1287, Apr. 2011. [Online]. Available: https://www.osapublishing.org/abstract.cfm?URI=ol-36-7-1287 [Cited on page 12.]

[54] H. P. S. Heng, C. Shu, W. Zheng, K. Lin, and Z. Huang, "Advances in real-time fiber-optic Raman spectroscopy for early cancer diagnosis: Pushing the frontier into clinical endoscopic applications," p. 32, 2020. [Cited on pages xiii, 13, 14, and 15.]

[55] E. Cordero, I. Latka, C. Matthäus, I. W. Schie, and J. Popp, "In-vivo Raman spectroscopy: from basics to applications," *Journal of Biomedical Optics*, vol. 23, p. 24, 2018. [Cited on pages 13 and 15.]

[56] H. P. Buschman, E. T. Marple, M. L. Wach, B. Bennett, T. C. Bakker Schut, H. A. Bruining, A. V. Bruschke, A. van der Laarse, and G. J. Puppels, "In Vivo Determination of the Molecular Composition of Artery Wall by Intravascular Raman Spectroscopy," *Analytical Chemistry*, vol. 72, no. 16, pp. 3771–3775, Aug. 2000, publisher: American Chemical Society. [Online]. Available: https://doi.org/10.1021/ac000298b [Cited on page 13.]

[57] M. Jermyn, J. Desroches, J. Mercier, K. St-Arnaud, M.-C. Guiot, K. Petrecca, and F. Leblond, "Neural networks improve brain cancer detection with Raman spectroscopy in the presence of light artifacts," S. J. Madsen, V. X. D. Yang, E. D. Jansen, Q. Luo, S. K. Mohanty, and N. V. Thakor, Eds., San Francisco, California, United States, Mar. 2016, p. 96900B. [Online]. Available: http://proceedings.spiedigitallibrary.org/proceeding.aspx?doi=10.1117/12.2208892 [Cited on pages xiii and 14.]

[58] D. Pappas, B. W. Smith, and J. D. Winefordner, "Raman spectroscopy in bioanalysis," p. 14, 2000. [Cited on page 15.]

[59] Z. Huang, H. Zeng, I. Hamzavi, D. I. McLean, and H. Lui, "Rapid near-infrared Raman spectroscopy system for real-time in vivo skin measurements,"

Optics Letters, vol. 26, no. 22, p. 1782, Nov. 2001. [Online]. Available: https://www.osapublishing.org/abstract.cfm?URI=ol-26-22-1782

[60] A. S. Haka, Z. Volynskaya, and J. A. Gardecki, "In vivo Margin Assessment during Partial Mastectomy Breast Surgery Using Raman Spectroscopy," *Cancer Res*, p. 8, 2006.

[61] S. Teh, W. Zheng, K. Ho, M. Teh, K. Yeoh, and Z. Huang, "Diagnostic potential of near-infrared Raman spectroscopy in the stomach: differentiating dysplasia from normal tissue," *Molecular Diagnostics*, p. 9, 2008.

[62] M. S. Bergholt, W. Zheng, K. Lin, K. Y. Ho, M. Teh, K. G. Yeoh, J. B. Y. So, and Z. Huang, "In vivo diagnosis of gastric cancer using Raman endoscopy and ant colony optimization techniques," *Int. J. Cancer*, p. 8, 2011.

[63] L. M. Almond, J. Hutchings, G. Lloyd, H. Barr, N. Shepherd, J. Day, O. Stevens, S. Sanders, M. Wadley, N. Stone, and C. Kendall, "Endoscopic Raman spectroscopy enables objective diagnosis of dysplasia in Barrett's esophagus," p. 9, 2014.

[64] A. Taketani, R. Hariyani, M. Ishigaki, B. B. Andriana, and H. Sato, "Raman endoscopy for the in situ investigation of advancing colorectal tumors in live model mice," p. 8, 2013.

[65] J. Wang, K. Lin, W. Zheng, K. Y. Ho, M. Teh, K. G. Yeoh, and Z. Huang, "Comparative study of the endoscope-based bevelled and volume fiber-optic Raman probes for optical diagnosis of gastric dysplasia in vivo at endoscopy," p. 8, 2015.

[66] S. Cui, S. Zhang, and S. Yue, "Raman Spectroscopy and Imaging for Cancer Diagnosis," *Journal of Healthcare Engineering*, vol. 2018, p. 8619342, Jun. 2018. [Online]. Available: https://www.ncbi.nlm.nih.gov/pmc/articles/PMC6011081/ [Cited on page 15.]

[67] "Thorlabs, Inc. - Your Source for Fiber Optics, Laser Diodes, Optical Instrumentation and Polarization Measurement & Control." [Online]. Available: https://www.thorlabs.com/ [Cited on pages xiii, xiv, 18, 33, 47, and 48.]

[68] E. Udd and W. B. S. Jr, *Fiber Optic Sensors: An Introduction for Engineers and Scientists*. John Wiley & Sons, Jul. 2011, google-Books-ID: FDs850m70_gC. [Cited on page 23.]

[69] D. Dantas, "Espetroscopia de Raman para aplicações Biomédicas," Ph.D. dissertation, Jul. 2019. [Cited on page 39.]

[70] D. Dantas, L. Soares, S. Novais, R. Vilarinho, J. A. Moreira, S. Silva, O. Fraz, and J. Reis, "Discrimination of Benign and Malignant Lesions in Canine Mammary Tissue Samples Using Raman Spectroscopy: A Pilot Study," p. 16, 2020. [Cited on page 39.]